receptor positions change between two trees we employed a delta-delta plot.

Delta-Delta plots

The delta-delta plot reveals how receptor locations behave globally with respect to the median of all receptors. It was used to visualize the differences in location of each receptor in sequence space and in substructure space. This plot is an adaptation from the delta-delta plot in Garr *et al.* [59]. It is a new way of tree comparison, which visualizes the differences among trees graphically, as opposed to the sole calculation of a numerical distance between two trees which is not trivial to interpret. For each receptor, the mean distance of that receptor to all other receptors was calculated. This value was plotted in a scatter plot, with each axis representing the mean distance of the respective node in one of the trees. The interpretation of this plot is as follows. Along both axes, receptors plotted far from the origin are, on average, more distant from the rest of the group, while receptors plotted close to the origin were closer to the rest of receptors. Receptors plotted near the diagonal do not change much in their mean distance to other receptors when going from one tree to the other (since they are close to the X = Y diagonal). Receptors plotted above or below the diagonal have different average distance to the other receptors between trees. For instance, consider a delta-delta plot that plots a substructure tree along the x-axis and a sequence tree along the y-axis. If a receptor is plotted above the diagonal, the mean distance of that receptor to the other receptors is larger in the sequence tree than the substructure tree; for receptors plotted below the diagonal, the opposite is true.

Validation

Leave-one-out validation

This experiment is repeated for every receptor (the 'orphan receptor') by temporarily removing ligands of this receptor from the dataset and predicting the position of molecules of this class in the substructure tree. A molecule from the left-out class is a hit when it is predicted to belong to one of the closest classes in sequence space. The closest classes in sequence space are found using the distance matrix from the multiple sequence alignment. Prediction of the class of a molecule is based on the Euclidean distance in substructure space. This distance is calculated as follows: for each substructure, the square of the difference between the relative frequency in a class and the molecule is calculated. The relative frequency of a substructure in a molecule is either 0 for absence, or 1 for presence of the substructure. The square root of the sum of all squared differences is the Euclidean distance between a molecule and a class. The area under the curve (AUC) of the receiver operating characteristic (ROC) plot served as a quality measure of the predictions for a class.

Instead of repeating the substructure mining for every left-out class, a lookup table of substructure occurrence was used. This table related all generated substructures with all molecules in which they occurred. Substructures that had a frequency just above the support threshold in the left-out class were not considered when analysis was performed for molecules of this class.

Additional material

Additional file 1 Phylogenetic trees based on 7TM domain and selected residues. Phylogenetic trees based on 7TM domain and selected residues. Two sequence-based phylogenetic trees for the set of Class A GPCRs used in this study: the phylogenetic tree based on the multiple sequence alignment of the 7TM domain and the phylogenetic tree based on 30 selected residues described in Surgand *et al.* [15]. Subfamilies are color-coded according to ligand type whereby the broad ligand types applied by in Gloriam *et al.* [17] were used. Legend: red - receptor with aminergic ligands; pink - peptide ligands; green - lipid ligands; dark blue - purinergic P2Y ligands; light blue - adenosine ligands; brown - melatonin ligands.

Additional file 2 Plotted scores for the *leave-one-out* validation. Plotted scores for the *leave-one-out* validation. The complete set of plotted scores of identified ligands per number of closest neighbors (sequences). For each plot, receptors are ordered along the x-axis (labeled "Number of included receptors") in order of increasing distance in sequence space to the receptor under study. The y-axis (labeled "Ligands identified") indicates the cumulative number of retrieved ligands, normalized linearly to the interval [0;1]. The red curve indicates the number of active ligands that are retrieved when including all (closest) receptors that are listed along the x-axis up to that point. More specifically, the number of correctly predicted ligands is plotted against the number of closely related receptors on which the prediction was based. For example, the plot of the muscarinic acetylcholine receptor M_1 (CHRM1, third row, third plot from the left) displays a steeply rising curve near the origin, indicating that many of its ligands are retrieved using a small number of closest receptors. The blue diagonal illustrates recovery of ligands when performance is equal to random prediction. The relative area under the curve (AUC) of the red curve is stated at the bottom of each plot. An AUC above 0.5 indicates good performance, while poor performance is indicated by an AUC of 0.5 or below. The plots are sorted according to decreasing (relative) AUC.

Additional file 3 List of GPCRs used in this study. List of GPCRs used in this study. The list of GPCRs used in this study (Class A, excluding singletons). Only receptors that are human, non-olfactory, and not orphan, were used. For each receptor, the respective (sub) family, gene symbol, official IUPHAR name, and number of ligands are provided.

Authors' contributions

EH carried out the sequence alignments, frequent substructure mining, analysis and validation, and drafted the manuscript. JEP participated in design of the study and visualization methods, and implementation of analyses. MWB, JRL, and HWTV assisted in study design, interpretation of results, and drafting the manuscript. MTME was involved in algorithm design and data analysis. YO was involved in acquisition of data in GLIDA. APIJ and AB participated in study design and coordination and helped to draft the manuscript. All authors read and approved the final manuscript.

Acknowledgements

The authors thank all members of the Division of Medicinal Chemistry of the Leiden/Amsterdam Center for Drug Research at Leiden University for helpful discussions. In addition, the authors thank Bas Vroling from the CMBI, Radboud University, for his help with the sequence alignments.

Funding: This work was supported by the Dutch Top Institute Pharma, project number: D1-105.

Author Details
[1]Division of Medicinal Chemistry, Leiden/Amsterdam Center for Drug Research, Leiden University, Einsteinweg 55, 2333CC, The Netherlands, [2]Leiden Institute for Advanced Computer Science, University of Leiden, The Netherlands, [3]Department of PharmacoInformatics, Center for Integrative Education of Pharmacy Frontier, Graduate School of Pharmaceutical Sciences, Kyoto University, Kyoto, Japan and [4]Unilever Centre for Molecular Science Informatics, Department of Chemistry, University of Cambridge, Cambridge, UK

Received: 4 March 2010 Accepted: 10 June 2010
Published: 10 June 2010

References

1. Fredriksson R, Lagerstrom MC, Lundin L-G, Schioth HB: **The G-Protein-Coupled Receptors in the Human Genome Form Five Main Families. Phylogenetic Analysis, Paralogon Groups, and Fingerprints.** *Molecular Pharmacology* 2003, **63(6):**1256-1272.
2. Jacoby E, Bouhelal R, Gerspacher M, Seuwen K: **The 7 TM G-Protein-Coupled Receptor Target Family.** *Chem Med Chem* 2006, **1(8):**760-782.
3. Jaakola V-P, Griffith MT, Hanson MA, Cherezov V, Chien EYT, Lane JR, IJzerman AP, Stevens RC: **The 2.6 Angstrom Crystal Structure of a Human A2A Adenosine Receptor Bound to an Antagonist.** *Science* 2008:1164772.
4. Ballesteros J, Palczewski K: **G protein-coupled receptor drug discovery: Implications from the crystal structure of rhodopsin.** *Curr Opin Drug Discovery Dev* 2001, **4(5):**561-574.
5. Cherezov V, Rosenbaum DM, Hanson MA, Rasmussen SGF, Thian FS, Kobilka TS, Choi H-J, Kuhn P, Weis WI, Kobilka BK, *et al.*: **High-Resolution Crystal Structure of an Engineered Human β_2-Adrenergic G Protein Coupled Receptor.** *Science* 2007, **318(5854):**1258-1265.
6. Warne T, Serrano-Vega MJ, Baker JG, Moukhametzianov R, Edwards PC, Henderson R, Leslie AGW, Tate CG, Schertler GFX: **Structure of a β_1-adrenergic G-protein-coupled receptor.** *Nature* 2008, **454(7203):**486-491.
7. Klabunde T, Hessler G: **Drug Design Strategies for Targeting G-Protein-Coupled Receptors.** *Chem Bio Chem* 2002, **3(10):**928-944.
8. Balakin KV, Tkachenko SE, Lang SA, Okun I, Ivashchenko AA, Savchuk NP: **Property-Based Design of GPCR-Targeted Library.** *J Chem Inf Comput Sci* 2002, **42(6):**1332-1342.
9. Chang LCW, Spanjersberg RF, von Frijtag Drabbe-Künzel JK, Mulder-Krieger T, van den Hout G, Beukers MW, Brussee J, IJzerman AP: **2,4,6-Trisubstituted Pyrimidines as a New Class of Selective Adenosine A_1 Receptor Antagonists.** *J Med Chem* 2004, **47(26):**6529-6540.
10. Bywater R: **Privileged Structures in GPCRs.** In *GPCRs: From Deorphanization to Lead Structure Identification* Edited by: Bourne H, Horuk R, Kuhnke J, Michel H. Springer-Verlag; 2007:75-92.
11. Doddareddy MR, Westen GJPv, Horst Evd, Peironcely JE, Corthals F, IJzerman AP, Emmerich M, Jenkins JL, Bender A: **Chemogenomics: Looking at biology through the lens of chemistry.** *Statistical Analysis and Data Mining* 2009, **2(3):**149-160.
12. Bender A, Young DW, Jenkins JL, Serrano M, Mikhailov D, Clemons PA, Davies JW: **Chemogenomic data analysis: Prediction of small-molecule targets and the advent of biological fingerprints.** *Comb Chem High Throughput Screening* 2007, **10(8):**719-731.
13. Klabunde T: **Chemogenomic approaches to drug discovery: similar receptors bind similar ligands.** *Br J Pharmacol* 2007, **152(1):**5-7.
14. Kolakowski LFJ: **GCRDb: a G-protein-coupled receptor database.** *Recept Channels* 1994, **2:**1-7.
15. Surgand J-S, Rodrigo J, Kellenberger E, Rognan D: **A chemogenomic analysis of the transmembrane binding cavity of human G-protein-coupled receptors.** *Proteins: Struct, Funct, Bioinf* 2006, **62(2):**509-538.
16. Rasmussen SGF, Choi H-J, Rosenbaum DM, Kobilka TS, Thian FS, Edwards PC, Burghammer M, Ratnala VRP, Sanishvili R, Fischetti RF, *et al.*: **Crystal structure of the human β_2 adrenergic G-protein-coupled receptor.** *Nature* 2007, **450(7168):**383-387.
17. Gloriam DE, Foord SM, Blaney FE, Garland SL: **Definition of the G Protein-Coupled Receptor Transmembrane Bundle Binding Pocket and Calculation of Receptor Similarities for Drug Design.** *J Med Chem* 2009, **52(14):**4429-4442.
18. Bender A, Jenkins JL, Glick M, Deng Z, Nettles JH, Davies JW: **"Bayes Affinity Fingerprints" Improve Retrieval Rates in Virtual Screening and Define Orthogonal Bioactivity Space: When Are Multitarget Drugs a Feasible Concept?** *J Chem Inf Model* 2006, **46(6):**2445-2456.
19. Bender A, Scheiber J, Glick M, Davies JW, Azzaoui K, Hamon J, Urban L, Whitebread S, Jenkins JL: **Analysis of Pharmacology Data and the Prediction of Adverse Drug Reactions and Off-Target Effects from Chemical Structure.** *ChemMedChem* 2007, **2(6):**861-873.
20. Keiser MJ, Roth BL, Armbruster BN, Ernsberger P, Irwin JJ, Shoichet BK: **Relating protein pharmacology by ligand chemistry.** *Nat Biotech* 2007, **25(2):**197-206.
21. van der Horst E, Okuno Y, Bender A, IJzerman AP: **Substructure Mining of GPCR Ligands Reveals Activity-Class Specific Functional Groups in an Unbiased Manner.** *J Chem Inf Model* 2009, **49(2):**348-360.
22. Borgelt C, Berthold MR: **Mining Molecular Fragments: Finding Relevant Substructures of Molecules.** In *Proceedings of the 2002 IEEE International Conference on Data Mining: 2002* IEEE Computer Society; 2002:51-58.
23. Nijssen S, Kok JN: **A quickstart in frequent structure mining can make a difference.** In *Proceedings of the tenth ACM SIGKDD international conference on Knowledge discovery and data mining: 2004* ACM Press, New York, USA; 2004:647-652.
24. Foord SM, Bonner TI, Neubig RR, Rosser EM, Pin J-P, Davenport AP, Spedding M, Harmar AJ: **International Union of Pharmacology. XLVI. G Protein-Coupled Receptor List.** *Pharmacol Rev* 2005, **57(2):**279-288.
25. Horn F, Bettler E, Oliveira L, Campagne F, Cohen FE, Vriend G: **GPCRDB information system for G protein-coupled receptors.** *Nucl Acids Res* 2003, **31(1):**294-297.
26. Baker JG: **The selectivity of β-adrenoceptor antagonists at the human β_1, β_2 and β_3 adrenoceptors.** *Br J Pharmacol* 2005, **144(3):**317-322.
27. Van Zwieten PA, Doods HN: **Muscarinic receptors and drugs in cardiovascular medicine.** *Cardiovascular Drugs and Therapy* 1995, **9(1):**159-167.
28. Voigtländer U, Jöhren K, Mohr M, Raasch A, Tränkle C, Buller S, Ellis J, Höltje H-D, Mohr K: **Allosteric site on muscarinic acetylcholine receptors: identification of two amino acids in the muscarinic M2 receptor that account entirely for the M2/M5 subtype selectivities of some structurally diverse allosteric ligands in N-methylscopolamine-occupied receptors.** *Molecular Pharmacology* 2003, **64(1):**21-31.
29. Okuno Y, Tamon A, Yabuuchi H, Niijima S, Minowa Y, Tonomura K, Kunimoto R, Feng C: **GLIDA: GPCR ligand database for chemical genomics drug discovery database and tools update.** *Nucl Acids Res* 2008, **36(suppl_1):**D907-912.
30. Paolini GV, Shapland RHB, van Hoorn WP, Mason JS, Hopkins AL: **Global mapping of pharmacological space.** *Nat Biotech* 2006, **24(7):**805-815.
31. Cuisiat S, Bourdiol N, Lacharme V, Newman-Tancredi A, Colpaert F, Vacher B: **Towards a New Generation of Potential Antipsychotic Agents Combining D2 and 5-HT1A Receptor Activities.** *J Med Chem* 2007, **50(4):**865-876.
32. Lawrence AJ: **Optimisation of anti-psychotic therapeutics: a balancing act?** *Br J Pharmacol* 2007, **151(2):**161-162.
33. Bondensgaard K, Ankersen M, Thogersen H, Hansen BS, Wulff BS, Bywater RP: **Recognition of Privileged Structures by G-Protein Coupled Receptors.** *J Med Chem* 2004, **47(4):**888-899.
34. Schnur DM, Hermsmeier MA, Tebben AJ: **Are Target-Family-Privileged Substructures Truly Privileged?** *J Med Chem* 2006, **49(6):**2000-2009.
35. Abramovitz M, Adam M, Boie Y, Carrière M-C, Denis D, Godbout C, Lamontagne S, Rochette C, Sawyer N, Tremblay NM, *et al.*: **The utilization of recombinant prostanoid receptors to determine the affinities and selectivities of prostaglandins and related analogs.** *Biochim Biophys Acta, Mol Cell Biol Lipids* 2000, **1483(2):**285-293.
36. Pettipher R, Hansel TT, Armer R: **Antagonism of the prostaglandin D2 receptors DP1 and CRTH2 as an approach to treat allergic diseases.** *Nat Rev Drug Discov* 2007, **6(4):**313-325.
37. Wang S, Gustafson E, Pang L, Qiao X, Behan J, Maguire M, Bayne M, Laz T: **A Novel Hepatointestinal Leukotriene B4 Receptor. Cloning and Functional Characterization.** *J Biol Chem* 2000, **275(52):**40686-40694.
38. Yokomizo T, Izumi T, Chang K, Takuwa Y, Shimizu T: **A G-protein-coupled receptor for leukotriene B4 that mediates chemotaxis.** *Nature* 1997, **387(6633):**620-624.
39. Le Crom S, Kapsimali M, Barôme P-O, Vernier P: **Dopamine receptors for every species: Gene duplications and functional diversification in**

Craniates. *Journal of Structural and Functional Genomics* 2003, **3(1):**161-176.
40. Zhang J, Xiong B, Zhen X, Zhang A: **Dopamine D1 receptor ligands: where are we now and where are we going.** *Med Res Rev* 2009, **29(2):**272-294.
41. Roth BL, Sheffler D, Potkin SG: **Atypical antipsychotic drug actions: unitary or multiple mechanisms for 'atypicality'?** *Clinical Neuroscience Research* 2003, **3(1-2):**108-117.
42. Coward DM: **General pharmacology of clozapine.** *The British Journal of Psychiatry Supplement* 1992:5-11.
43. Zakon HH: **Convergent Evolution on the Molecular Level.** *Brain, Behavior and Evolution* 2002, **59(5-6):**250-261.
44. Mestres J, Gregori-Puigjane E, Valverde S, Sole RV: **Data completeness--the Achilles heel of drug-target networks.** *Nat Biotech* 2008, **26(9):**983-984.
45. Bemis GW, Murcko MA: **The Properties of Known Drugs. 1. Molecular Frameworks.** *J Med Chem* 1996, **39(15):**2887-2893.
46. van der Horst E, IJzerman AP: **Computational Approaches to Fragment and Substructure Discovery and Evaluation.** In *Fragment-Based Drug Discovery: A Practical Approach* Edited by: Zartler ER, Shapiro J, Chichester M. West Sussex, U.K.: John Wiley & Sons, Ltd; 2008.
47. Bernasconi P, Min C, Galasinski S, Popa-Burke I, Bobasheva A, Coudurier L, Birkos S, Hallam R, Janzen WP: **A Chemogenomic Analysis of the Human Proteome: Application to Enzyme Families.** *J Biomol Screen* 2007, **12(7):**972-982.
48. **ChEMBL** [http://www.ebi.ac.uk/chembl/]
49. Roth BL, Lopez E, Beischel S, Westkaemper RB, Evans JM: **Screening the receptorome to discover the molecular targets for plant-derived psychoactive compounds: a novel approach for CNS drug discovery.** *Pharmacol Ther* 2004, **102(2):**99-110.
50. The UniProt Consortium: **The Universal Protein Resource (UniProt).** *Nucl Acids Res* 2008, **36(suppl_1):**D190-195.
51. Wheeler DL, Barrett T, Benson DA, Bryant SH, Canese K, Chetvernin V, Church DM, DiCuccio M, Edgar R, Federhen S, *et al.*: **Database resources of the National Center for Biotechnology Information.** *Nucl Acids Res* 2008:D13-D21.
52. Wishart DS, Knox C, Guo AC, Shrivastava S, Hassanali M, Stothard P, Chang Z, Woolsey J: **DrugBank: a comprehensive resource for in silico drug discovery and exploration.** *Nucl Acids Res* 2006, **34(suppl_1):**D668-672.
53. **GPCRDB** [http://www.gpcr.org/7tm/]
54. **GASTON** [http://www.liacs.nl/~snijssen/gaston/]
55. Wörlein M, Meinl T, Fischer I, Philippsen M: **A Quantitative Comparison of the Subgraph Miners MoFa, gSpan, FFSM, and Gaston.** *Knowledge Discovery in Databases: PKDD 2005* 2005:392-403.
56. Agrawal R, Srikant R: **Fast Algorithms for Mining Association Rules in Large Databases.** In *Proceedings of the 20th International Conference on Very Large Data Bases: September 12 - 15 1994* Morgan Kaufmann Publishers, San Francisco, CA; 1994:487-499.
57. Felsenstein J: **PHYLIP (Phylogeny Inference Package) version 3.6. Distributed by the author. Department of Genome Sciences, University of Washington, Seattle.** 2005.
58. Tamura K, Dudley J, Nei M, Kumar S: **MEGA4: Molecular Evolutionary Genetics Analysis (MEGA) Software Version 4.0.** *Mol Biol Evol* 2007, **24(8):**1596-1599.
59. Garr CD, Peterson JR, Schultz L, Oliver AR, Underiner TL, Cramer RD, Ferguson AM, Lawless MS, Patterson DE: **Solution Phase Synthesis of Chemical Libraries for Lead Discovery.** *J Biomol Screen* 1996, **1(4):**179-186.

doi: 10.1186/1471-2105-11-316
Cite this article as: van der Horst *et al.*, A novel chemogenomics analysis of G protein-coupled receptors (GPCRs) and their ligands: a potential strategy for receptor de-orphanization *BMC Bioinformatics* 2010, **11**:316

Biochimie 92 (2010) 665–675

Contents lists available at ScienceDirect

Biochimie

journal homepage: www.elsevier.com/locate/biochi

Research paper

Expression profiling of cumulus cells reveals functional changes during ovulation and central roles of prostaglandin EP2 receptor in cAMP signaling

Shigero Tamba [a], Rieko Yodoi [a], Kazushi Morimoto [a], Tomoaki Inazumi [a], Mamiko Sukeno [a], Eri Segi-Nishida [a,b], Yasushi Okuno [b], Gozoh Tsujimoto [c], Shuh Narumiya [d], Yukihiko Sugimoto [a,e,*]

[a] Department of Physiological Chemistry, Kyoto University Graduate School of Pharmaceutical Sciences, Sakyo-ku, Kyoto 606-8501, Japan
[b] Department of Systems Bioscience for Drug Discovery, Kyoto University Graduate School of Pharmaceutical Sciences Sakyo-ku, Kyoto 606-8501, Japan
[c] Department of Genomic Drug Discovery Science Kyoto University Graduate School of Pharmaceutical Sciences, Sakyo-ku, Kyoto 606-8501, Japan
[d] Department of Pharmacology, Faculty of Medicine, Kyoto University, Sakyo-ku, Kyoto 606-8501, Japan
[e] Department of Pharmaceutical Biochemistry, Kumamoto University Graduate School of Pharmaceutical Sciences, Kumamoto 862-0973, Japan

ARTICLE INFO

Article history:
Received 30 September 2009
Accepted 13 April 2010
Available online 20 April 2010

Keywords:
Reproduction
Ovulation
Prostanoid
Gonadotropin
Gene expression profile

ABSTRACT

To understand the role of prostaglandin (PG) receptor EP2 (*Ptger2*) signaling in ovulation and fertilization, we investigated time-dependent expression profiles in wild-type (WT) and *Ptger2*$^{-/-}$ cumuli before and after ovulation by using microarrays. We prepared cumulus cells from mice just before and 3, 9 and 14 h after human chorionic gonadotropin injection. Key genes including cAMP-related and epidermal growth factor (EGF) genes, as well as extracellular matrix- (ECM-) related and chemokine genes were up-regulated in WT cumuli at 3 h and 14 h, respectively. *Ptger2* deficiency differently affected the expression of many of the key genes at 3 h and 14 h. These results indicate that the gene expression profile of cumulus cells greatly differs before and after ovulation, and in each situation, PGE_2-EP2 signaling plays a critical role in cAMP-regulated gene expression in the cumulus cells under physiological conditions.

1. Introduction

Ovulation and fertilization are key processes in mammalian female reproduction, which is highly regulated by pituitary gonadotropins, follicle-stimulating hormone (FSH) and luteinizing hormone (LH). These hormones induce a number of preovulatory processes including follicular development, oocyte maturation, cumulus expansion, and rupture of antral follicles [1]. The ovulated eggs are directed to the oviduct, and timely interaction between an egg and a sperm then leads to successful fertilization [2]. Undoubtedly, these processes are initiated by gonadotropins, but recent studies have shown that many of the actions of gonadotropins are mediated by various mediators produced locally within the follicles [3].

The cumulus oophorus is composed of a group of closely associated granulosa cells that surround the oocyte in the antral follicle, and are collectively called cumulus cells [4]. In response to a luteinizing hormone (LH) surge, the cumulus cells start to produce extracellular matrix (ECM) components, which are deposited into the intercellular space and are stabilized by accessory proteins. This phenomenon is called cumulus expansion. A major component of the ECM produced by the cumulus cells is hyaluronan, which provides the viscoelastic properties of the cumulus oophorus. Other proteoglycans and glycoproteins, such as fibronectin, laminin and type IV collagen, are also produced by cumulus cells. The expanded cumulus oophorus (cumulus cells and ECM) forms a tight complex with an oocyte, and is ovulated together as the cumulus–oocyte complex (COC). During ovulation, the cumulus oophorus protects the oocyte from mechanical stress and from proteolytic enzymes present in the follicle and oviduct, and directs the oocyte into the oviduct by facilitating its capture by the ciliated epithelial cells of the infundibulum and its transport to the fertilization site [5]. In the oviduct, the cumulus oophorus facilitates the access of the sperm to the oocyte by trapping and selecting sperms for successful fertilization [6]. Thus, complex formation of the oocyte, cumulus cells and ECM is essential for successful fertilization in the oviduct [7]. Indeed, recent studies using mice null of several hyaluronan binding proteins show that the cumulus ECM is required for successful fertilization *in vivo*; female mice deficient in these molecules are sterile due to a loss of the cumulus and ECM [8–11]. Although the importance of the cumulus and ECM has thus been acknowledged, gonadotropin-induced changes in gene expression profiles of cumulus cells have not been analyzed in detail.

One of the major mediators in response to the gonadotropins is prostaglandin (PG) E_2, an arachidonate metabolite in the ovary. It has

* Corresponding author. Department of Pharmaceutical Biochemistry, Kumamoto University Graduate School of Pharmaceutical Sciences, Kumamoto 862-0973, Japan. Fax: +81 96 372 7182.
E-mail address: ysugi@kumamoto-u.ac.jp (Y. Sugimoto).

0300-9084/$ – see front matter © 2010 Published by Elsevier Masson SAS.
doi:10.1016/j.biochi.2010.04.006

been shown that cyclooxygenase-2 (COX-2; *Ptgs2*) is responsible for the production of PGE_2 in the ovary and plays a critical role in multiple reproduction processes; *Ptgs2*$^{-/-}$ female mice showed a reduction in ovulation number, and severe failure in fertilization as well as implantation [12]. PGE_2 exerts its actions by acting on four subtypes of the PGE receptor, EP1 to EP4 (*Ptger1* to *Ptger4*). Among these four subtypes, the mice lacking the EP2 receptor (*Ptger2*), which is expressed in cumulus cells, exhibit impaired ovulation and fertilization due to defects in cumulus cell function [13]. We recently explored the molecular basis of this impaired fertilization in *Ptger2*$^{-/-}$ mice, and demonstrated 1) increased gene expression of chemokines such as *Ccl2*, *Ccl7* and *Ccl9* in *Ptger2*$^{-/-}$ cumulus cells compared with wild-type (WT) cells and that 2) PGE_2-EP2 signaling negatively regulates such chemokine-induced integrin engagement to the ECM and allows sperm penetration through the cumulus ECM [14,15]. However, the mechanisms responsible for the impaired ovulation in *Ptger2*$^{-/-}$ mice remains unknown and it is still possible that unidentified factors other than chemokine signaling are also involved in the process of impaired fertilization in *Ptger2*$^{-/-}$ mice.

Global gene expression profile analysis is a powerful tool for discovering new pathways involved in various biological processes including ovulation and fertilization. Indeed, several studies to date have reported changes in cumulus gene expression in response to gonadotropins, but these studies were based on expression changes in heterogenous samples such as whole ovaries or COCs [16–18]. Microdissection of cumulus cells under stereoscopic examination yields only ~10 ng of total RNA per mouse, and it is extremely difficult to examine gene expression profiles starting with such a small quantity of cumulus RNA. However, obtaining the gene expression profiles of genuine cumulus cells will be ideal for investigating new cumulus functions and the effects of *Ptger2* deficiency on cumulus cell function. We therefore established an amplification protocol for cumulus RNA, which enabled us to reproducibly detect changes in cumulus expression profiles. We here report the temporal changes in cumulus gene expression profiles in WT mice and the effect of *Ptger2* deficiency on these changes.

2. Materials and methods

2.1. Animals and hormone treatment

Female C57BL/6 mice (3 weeks of age) purchased from Japan SLC were used as WT mice. *Ptger2*$^{-/-}$ mice were obtained as previously described [13]. *Ptger2*$^{-/-}$ mice, backcrossed for more than 10 generations to C57BL/6 mice, were maintained on a 12-h light/dark cycle under specific pathogen-free conditions. Follicular growth and ovulation were stimulated in mice at 3–4 weeks of age by the following hormonal regimen: intraperitoneal (ip) injection of 5 IU PMSG followed 48 h later by ip injection of 5 IU hCG. All experimental procedures were approved by the Committee on Animal Research of Kyoto University Graduate School of Pharmaceutical Sciences.

2.2. Preparation of total RNA from cumulus cells

WT and *Ptger2*$^{-/-}$ mice were sacrificed at different time points (0, 3, 9, 14 h) after hCG injection. At time points before ovulation (at post-hCG, 0, 3 or 9 h), eight ovaries from four mice were collected and large antral follicles visible on the surface of the ovary were ruptured using a 30-gauge needle allowing the COCs to flow out into phosphate-buffered saline containing 0.3% BSA (0.3% BSA/PBS). Fourteen to 16 COCs were isolated from each of four animals for each time point. Using glass capillaries, cumulus cells and the oocyte were surgically stripped, and cumulus cells were removed from the oocytes. At 14 h after hCG, the COCs were collected from the ampullary of the oviducts and treated with 0.1% hyaluronidase (Sigma–Aldrich) to strip the COCs of cumulus cells. The procedures including collection of COCs and isolation of cumulus cells for each time point were performed within 1 h. For array analysis, cumulus cells from five animals were pooled, and RNA was extracted for each time point. For real-time reverse transcription- (RT-) PCR analysis, the cumulus cells were collected per animal, and RNA was extracted separately for each animal. Total RNA of cumulus cells was then obtained with an RNeasy Mini Kit (QIAGEN). The RNA was stored at −80 °C until use.

2.3. Oligonucleotide array and data analysis

The complete procedure of array analysis of multiple RNA samples including WT and *Ptger2*$^{-/-}$ group (four time points each) were performed simultaneously. One hundred nanograms of total RNA for each group was used to generate double-strand cDNA with the T7-oligo $(dT)_{24}$ primer (GE Healthcare Bioscience) according to the GeneChip Eukaryotic Small Sample Target Labeling Assay Version I protocol. After second-strand synthesis, *in vitro* transcription was performed using a MEGAscript High Yield Transcription kit (Ambion). The cRNA synthesized after the first cycle of *in vitro* transcription was then used as a template in a second cycle of first-strand cDNA synthesis with random primers (Invitrogen Life Technologies). Then, the second-strand synthesis was

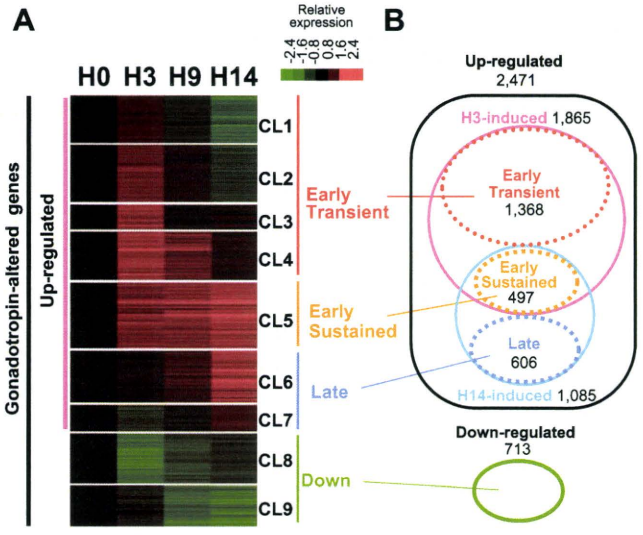

Fig. 1. Gonadotropin-primed changes in gene expression in WT cumulus cells. (A) Representation of mRNA expression levels of WT cumulus cells at the indicated hours after human chorionic gonadotropin (hCG) injection compared with just before the hCG injection (H0). COCs were isolated from the ovary at post-hCG 3 (H3) and 9 h (H9), or isolated from the oviduct at post-hCG 14 h (H14). The cumulus cells were then collected, and total RNA at each time point was subjected to oligonucleotide microarray analysis after RNA amplification. Each gene is represented by a single row. The colors represent the ratio of hybridization measurements between corresponding time points and H0 profiles, according to the scale shown. (B) Genes are placed in groups corresponding to pairwise overlaps shown in the accompanying Venn diagrams. (C) Schematic representation of early and late gene expression profiles based on the expression kinetics of gonadotropin-responsive genes. Transient and sustained patterns are also shown. Down-regulated genes (Down) were placed according to the patterns corresponding to clusters 8 (CL8) and 9 (CL9). Stages of the cumulus cell life cycle are shown below: cumulus cells undergo proliferation, maturation, and expansion to secret ECM components; the cells exposed to pro-inflammatory factors then undergo ovulation; and the ovulated cumulus cells are directed to the oviduct and transferred into the ampulla, followed by adaptive changes of cumulus cells to the oviductal environment. Blue and pink colors reflect the difference in ECM components before and after ovulation. (D) Genes regulated at different times in response to gonadotropin are listed according to their functional category.

C

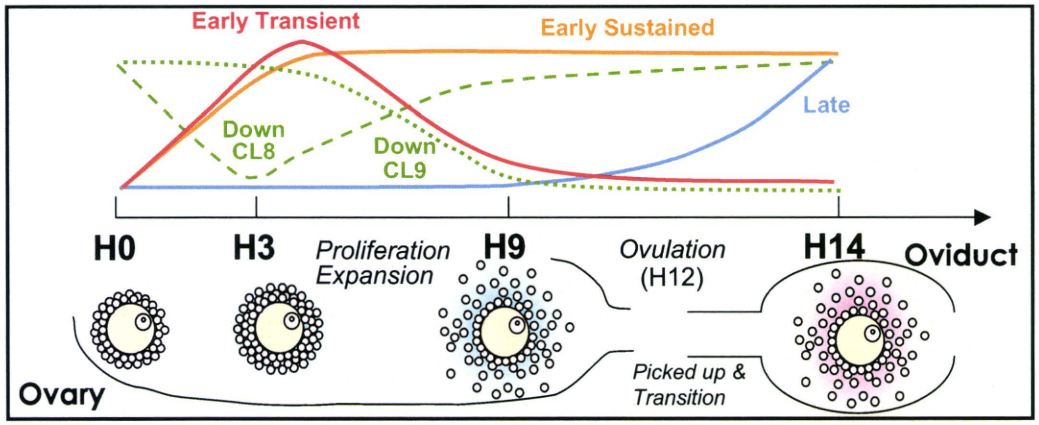

D

Functional Category	Up			Down	
	Early Transient (CLs 1-4)	Early Sustained (CL5)	Late (CLs 6-7)	Down (CL8)	Down (CL9)
PG	Ptges, Ptger4, Pla2g4a, Pla2g12, Ptger2	Ptgs2			Hpgd, Ptgis
cAMP signaling	Crem, Nmu, Rgs10, Prkar1a, Prkab1, Akap2			Akap8	
Growth factor	Areg, Ereg, Btc, Vegfa, Ephb4, Pparg, Efnb2, Kitl	Bmp6	Vegfc,Bmp1, Numb, Bnip3		Inhbb, Inhba
Steroid hormone	Star, Idi1, Cyp51, Hmgcs1, Hmgcr, Hsd3b1			Nr5a1, Irf6	Esr2, Cyp2s1
Immune cell	Ifi202b	Il1r1, Ifrd1	Il10rb, Cfh, Ifi204, S100a8, Il13ra1, Il1rn	Btk	
Chemokine	Cx3cl1, Cxcr4		Ccr5, Cxcl2, Ccl9, Ccl2, Ccr1		
ECM	Ptx3, Has2, Piga, Itga2, Icam1	Tnfaip6, Mglap, Alcam, Anxa2, Sdc1, Itgb5	Tnc, Anxa1, Vcl, Ovgp1, Mbp, Sparc, Anxa11, Gp49a, Pcdh7, Mmp11, Cdh5, Fn1, Timp3, Itgb1, Sdc4, Lamc1, Mmp14	Vim, Timp1	
Collagen			Col4a1, Col18a1, Col4a2, Col6a1		
Actin Cytoskeleton	Bex1	Actr10, Capza2, Capg, Actn1, Actg			
Cell cycle	Ccng2, Cdkn1a, Cdk4				Ccdn2, Cdc6
Other	Ndufb8, Ndufb10, Ndufb9, Ndufa2, Ndufa7 Rpl36, Rps16, Rpl10a, Rpl19, Rpl26 Procr	Acsl4	Abcb1b, Cyp1b1	Eif4e, Snx17	

Fig. 1. (*continued*).

performed in the presence of the oligo(dT)$_{24}$ primer. For the second-strand cDNA synthesis, *in vitro* transcription was performed using an ENZO BioArray HighYield RNA Transcription Labeling kit (ENZO Diagnostics) to generate biotin-labeled cRNA. For each sample, 20 μg of the cRNA product was fragmented and hybridized for 18 h into Affymetrix GeneChip Murine Genome U74Av2 arrays. Each array was washed and stained with streptavidin-phycoerythrin (Molecular Probes) and scanned with the GeneArray Scanner (Agilent Technologies) according to the GeneChip Expression Analysis Technical Manual procedure (Affymetrix). We used the robust multi-array average (RMA) expression measure for log transformation ($\log_2$) and normalization of the multiple GeneChip data (eight array data including four time points per genotype) [19,20]. The RMA measures were calculated using the R package program, which is freely available on the internet (http://www.bioconductor.org). After normalization of eight array data, we selected genes in which the maximum minus minimum values between WT at 48 h after PMSG injection and any of the time points of WT were greater than 2 (a 2-fold change). For the four WT array data, using the *k*-means clustering algorithm, these genes were classified into nine clusters on the basis of the similarity of their temporal expression profiles [20,21]. All array data have been deposited in the Gene Expression Omnibus (GSE20439).

2.4. Real time RT-PCR

For real-time RT-PCR analysis, cumulus cells and mural granulosa cells isolated from each animal were pooled and subjected to RNA

Table 1
Genes induced at H3 after gonadotropin stimulation (CLs 1–5). The list represents genes in which expression levels were up-regulated only at H3 and then decreased (CLs 1–3), and genes in which expression levels were up-regulated both at H3 and H9 and then decreased (CL4) or genes in which expression levels were up-regulated at H3 and then sustained until H14 (CL5). The change in the expression level of each gene at each time point is indicated as a logarithm of the fold-change versus the expression level at H0, and the difference in the expression level of each gene in the cells at H3 versus at H0 are shown as a logarithm of the fold-change in bold. Representative genes with the largest changes are shown. ID, Affymetrix ID number.

Symbol	CL	Gene title	H3/H0 log2(fold)	H9/H0 log2(fold)	H14/H0 log2(fold)	ID
PG-related genes						
Ptgs2	5	prostaglandin-endoperoxide synthase 2	**7.4**	6.0	5.2	104647_at
Ptger4	3	prostaglandin E receptor 4 (subtype EP4)	**2.5**	0.2	0.1	103362_at
Pla2g4a	4	phospholipase A2 group IVA (cytosolic Ca-dependent)	**1.8**	1.5	0.5	99513_at
Ptges	1	prostaglandin E synthase	**1.7**	−0.7	−1.1	104406_at
Pla2g12	2	phospholipase A2 group XII	**1.1**	0.0	−0.3	104342_i_at
Ptger2	3	prostaglandin E receptor 2 (subtype EP2)	**1.0**	0.5	0.5	98768_at
cAMP-related genes						
Crem	3	cAMP responsive element modulator	**4.7**	1.4	0.9	160526_s_at
Nmu	4	neuromedin	**2.4**	1.9	0.3	161032_i_at
Rgs10	3	regulator of G-protein signaling 10	**2.2**	0.3	0.1	160629_at
Prkar1a	3	protein kinase cAMP dependent regulatory I alpha	**1.4**	0.3	0.5	96852_at
Prkab1	3	protein kinase AMP-activated beta 1 non-catalytic	**1.2**	0.3	−0.1	160808_at
Akap2	3	A kinase (PRKA) anchor protein 2	**1.1**	0.2	−0.2	101435_at
Growth factor-related genes						
Areg	3	amphiregulin	**6.6**	2.8	0.7	99915_at
Ereg	4	epiregulin	**3.0**	2.0	1.0	98802_at
Btc	4	betacellulin	**2.7**	1.3	0.5	95310_at
Vegfa	3	vascular endothelial growth factor A	**2.4**	0.4	1.2	103520_at
Ephb4	4	Eph receptor B4	**2.3**	0.7	0.0	98446_s_at
Pparg	1	peroxisome proliferator activated receptor gamma	**1.5**	−0.9	−1.8	97926_s_at
Efnb2	4	ephrin B2	**1.5**	1.5	0.8	160857_at
Bmp6	5	bone morphogenetic protein 6	**1.4**	0.2	1.3	161028_at
Kitl	1	kit ligand	**1.0**	−0.8	−0.5	99577_at
Steroid hormone-related genes						
Star	4	steroidogenic acute regulatory protein	**4.5**	3.5	2.2	92213_at
Idi1	4	isopentenyl-diphosphate delta isomerase	**2.0**	1.5	−0.2	96269_at
Cyp51	4	cytochrome P450 51	**1.9**	1.4	0.5	94916_at
Hmgcs1	4	3-hydroxy-3-methylglutaryl-Coenzyme A synthase 1	**1.8**	2.4	0.9	94325_at
Hmgcr	4	3-hydroxy-3-methylglutaryl-Coenzyme A reductase	**1.6**	1.8	1.0	104285_at
Hsd3b1	4	hydroxysteroid dehydrogenase-1 delta<5>-3-beta	**1.5**	1.2	1.1	103072_at
Immune cell-related genes						
Ifi202b	3	interferon activated gene 202B	**3.1**	0.2	0.0	94774_at
Il1r1	5	interleukin 1 receptor type I	**2.8**	1.3	2.8	93914_at
Ifrd1	5	interferon-related developmental regulator 1	**2.2**	2.9	1.9	160092_at
Cx3cl1	1	chemokine (C-X3-C motif) ligand 1	**1.4**	−0.2	−0.6	98008_at
Cxcr4	4	chemokine (C-X-C motif) receptor 4	**1.2**	1.5	0.4	102794_at
ECM-related genes						
Ptx3	4	pentraxin related gene	**4.6**	4.1	2.0	92731_at
Has2	3	hyaluronan synthase 2	**4.3**	1.3	0.0	98865_at
Tnfaip6	5	tumor necrosis factor alpha induced protein 6	**3.8**	3.6	3.8	98474_r_at
Mglap	5	matrix gamma-carboxyglutamate (gla) protein	**3.8**	4.0	3.4	93866_s_at
Alcam	5	activated leukocyte cell adhesion molecule	**2.7**	4.0	3.8	104407_at
Anxa2	5	annexin A2	**2.0**	2.5	3.2	100569_at
Piga	1	phosphatidylinositol glycan class A	**1.9**	−0.5	−0.6	92304_at
Sdc1	5	syndecan 1	**1.9**	2.5	2.4	96033_at
Itga2	3	integrin alpha 2	**1.7**	0.2	−0.3	98834_at
Itgb5	5	integrin beta 5	**1.2**	1.1	0.9	100601_at
Icam1	1	intercellular adhesion molecule	**1.0**	−0.1	−0.4	104037_at
Actin cytoskeleton-related genes						
Bex1	2	brain expressed gene 1	**3.6**	1.1	−0.4	93020_at
Actr10	5	ARP10 actin-related protein 10 homolog	**1.7**	1.8	1.5	95097_at
Capza2	5	cap protein (actin filament) muscle Z-line alpha 2	**1.2**	0.8	2.0	98127_at
Capg	5	capping protein (actin filament) gelsolin-like	**1.1**	1.6	1.3	160106_at
Actn1	5	actinin alpha 1	**1.1**	1.4	2.7	104579_r_at
Actg	5	actin gamma cytoplasmic	**1.0**	1.3	1.0	96573_at
Cell cycle-related genes						
Ccng2	3	cyclin G2	**1.8**	−0.3	0.9	98478_at
Cdkn1a	3	cyclin-dependent kinase inhibitor 1A (P21)	**1.8**	0.5	0.6	98067_at
Cdk4	2	cyclin-dependent kinase 4	**1.2**	−0.2	−0.4	101017_at
NADH dehydrogenase genes						
Ndufb8	2	NADH dehydrogenase (ubiquinone) 1 beta 8	**2.1**	1.0	−0.9	93581_at
Ndufb10	2	NADH dehydrogenase (ubiquinone) 1 beta 10	**2.1**	1.2	−0.6	101525_at
Ndufb9	2	NADH dehydrogenase (ubiquinone) 1 beta 9	**1.3**	0.6	−0.3	100079_at
Ndufa2	2	NADH dehydrogenase (ubiquinone) 1 alpha 2	**1.2**	0.8	−0.4	96280_at
Ndufa7	2	NADH dehydrogenase (ubiquinone) 1 alpha 7	**1.2**	0.5	−0.1	95652_at

Table 1 (*continued*)

Symbol	CL	Gene title	H3/H0 log2(fold)	H9/H0 log2(fold)	H14/H0 log2(fold)	ID
Ribosomal protein genes						
Rpl36	2	ribosomal protein L36	**1.8**	1.4	−1.7	92628_at
Rps16	2	ribosomal protein S16	**1.6**	1.3	−0.5	97647_at
Rpl10a	2	ribosomal protein L10A	**1.4**	0.5	−1.0	100711_at
Rpl19	2	ribosomal protein L19	**1.3**	0.6	−0.9	97483_at
Rpl26	2	ribosomal protein L26	**1.3**	1.2	−0.8	100729_at
Other genes						
Procr	4	protein C receptor endothelial	**5.5**	4.4	2.8	98018_at
Acsl4	5	acyl-CoA synthetase long-chain family member 4	**3.2**	3.6	4.3	102381_at

extraction, and total RNA (10 ng) was subjected to the RT reaction with a SuperScript First-Strand Synthesis Kit according to manufacturer's instructions (Invitrogen Life Technologies). The relative expression levels of genes representative for each cluster (*Piga*, *Bex1*, *Crem*, *Star*, *Acsl4*, *Mbp*, *Cyp1b1*, *Akap8*, and *Ccdn2*), or genes showing differential expression between WT and *Ptger2*$^{-/-}$ cumuli (*Bex1*, *Procr*, *Cyp1b1*, *Mbp*, *C1qb* and *Ccl2*), or 6 selected genes (*Crem*, *Ptgs2*, *Ptger4*, *Areg*, *Ereg* and *Btc*) were monitored with a LightCycler and real-time detection system (Roche Diagnostics) using Fast Start DNA Master SYBR Green I according to the manufacturer's instructions. Crossing point values were acquired by using the second derivative maximum method. The expression level of each gene was quantified using external standardized dilutions. Relative expression levels of target genes between samples were normalized by those of

Table 2
Genes induced at a later time point upon gonadotropin stimulation (CLs 6–7). The list represents genes in which expression levels were low both at H3 and H9 but up-regulated at H14 (CLs 6-7). The change in the expression level of each gene at each time point is indicated as a logarithm of the fold-change versus the expression level at H0, and the difference in the expression level of each gene in the cells at H14 versus at H0 are shown as a logarithm of the fold-change in bold. Representative genes with the largest changes are shown. ID, Affymetrix ID number.

Symbol	CL	Gene title	H3/H0 log2(fold)	H9/H0 log2(fold)	H14/H0 log2(fold)	ID
Growth factor-related genes						
Vegfc	6	vascular endothelial growth factor C	0.1	0.2	**1.9**	94712_at
Numb	6	numb gene homolog (*Drosophila*)	0.1	0.4	**1.2**	161912_r_at
Bnip3	7	BCL2/adenovirus E1B19 kDa-interacting 1 NIP3	−1.2	−0.8	**1.2**	93836_at
Bmp1	6	bone morphogenetic protein 1	−0.4	0.2	**1.0**	92701_at
Immune-related genes						
Il10rb	6	interleukin 10 receptor beta	−0.4	1.3	**2.5**	99491_at
Cfh	6	complement component factor h	0.4	0.5	**1.9**	101853_f_at
Ifi204	6	interferon activated gene 204	0.5	−0.2	**1.5**	98465_f_at
S100a8	7	S100 calcium binding protein A8 (calgranulin A)	−0.4	−0.1	**1.4**	103448_at
Il13ra1	6	interleukin 13 receptor alpha 1	−0.6	0.4	**1.3**	103723_at
Il1rn	6	interleukin 1 receptor antagonist	−0.2	0.1	**1.2**	93871_at
Ccr5	6	chemokine (C-C motif) receptor 5	−0.1	0.0	**1.1**	161968_f_at
Cxcl2	7	chemokine (C-X-C motif) ligand 2	−0.6	−0.3	**0.8**	101160_at
Ccl9	7	chemokine (C-C motif) ligand 9	−0.5	−0.1	**0.8**	104388_at
Ccl2	6	chemokine (C-C motif) ligand 2	−0.2	−0.1	**0.7**	102736_at
Ccr1	6	chemokine (C-C motif) receptor 1	−0.2	0.1	**0.6**	99413_at
ECM-related genes						
Tnc	6	tenascin C	−0.1	1.5	**4.8**	162362_f_at
Anxa1	6	annexin A1	1.0	3.0	**4.1**	93038_f_at
Vcl	6	vinculin	1.2	1.6	**3.7**	94963_at
Ovgp1	6	oviductal glycoprotein 1	−0.7	−0.2	**3.4**	100521_at
Mbp	6	myelin basic protein	−0.1	1.0	**3.3**	96311_at
Sparc	6	secreted acidic cysteine rich glycoprotein	0.2	1.9	**3.0**	97160_at
Anxa11	6	annexin A11	−0.1	1.2	**2.8**	102815_at
Gp49a	6	glycoprotein 49 A	−0.1	0.1	**2.6**	100325_at
Pcdh7	6	protocadherin 7	−0.5	1.0	**2.2**	102280_at
Mmp11	6	matrix metalloproteinase 11	0.0	0.9	**2.0**	100016_at
Cdh5	6	cadherin 5	−0.2	1.8	**1.9**	104083_at
Fn1	6	fibronectin 1	0.6	0.3	**1.8**	92852_at
Timp3	6	tissue inhibitor of metalloproteinase 3	0.3	1.3	**1.7**	160519_at
Itgb1	6	integrin beta 1 (fibronectin receptor beta)	0.4	0.4	**1.7**	100124_r_at
Sdc4	6	syndecan 4	−0.2	0.3	**1.4**	98590_at
Lamc1	6	laminin gamma 1	−0.3	0.4	**1.1**	161706_f_at
Mmp14	7	matrix metalloproteinase 14	−1.0	0.9	**1.1**	160118_at
Collagen-related genes						
Col4a1	6	procollagen type IV alpha 1	0.2	3.1	**4.1**	101093_at
Col18a1	6	procollagen type XVIII alpha 1	−0.1	2.2	**3.1**	101881_g_at
Col4a2	6	procollagen type IV alpha 2	−0.3	1.0	**2.5**	101039_at
Col6a1	6	procollagen type VI alpha 1	−0.3	0.1	**1.8**	162459_f_at
Other genes						
Abcb1b	6	ATP-binding cassette sub-family B, member 1B	−0.5	2.9	**5.1**	93414_at
Cyp1b1	7	cytochrome P450, family 1, subfamily b, polypeptide 1	−1.1	0.1	**1.4**	99979_at

glyceraldehyde-3-phosphate dehydrogenase (*Gapdh*). Primer sequences for each gene are shown in Table 6. The specificity of each primer set was confirmed by checking the product size by gel electrophoresis and melting temperature.

2.5. Statistical analyses

Data are shown as means ± S.E.M. Comparison of two groups was analyzed by the Student's *t* test (*Ptger2*$^{-/-}$ *vs* WT). For comparison of more than two groups with comparable variances (Time course), one-way ANOVA was performed first. Then, the Dunnett or Tukey–Kramer test was used to evaluate the difference.

3. Results and discussion

3.1. Temporal changes in gene expression profiles of WT cumulus cells upon gonadotropin stimulation

We used oligonucleotide microarrays to investigate gonadotropin-induced gene expression profiles in WT cumulus cells before and after ovulation. Immature mice were primed with pregnant mare serum gonadotropin (PMSG) as an FSH-like stimulation. The COCs were isolated from mice 48 h after PMSG injection (H0) and from PMSG-primed mice exposed to human chorionic gonadotropin (hCG) as an LH-like stimulation for 3, 9 or 14 h (H3, H9 or H14, respectively). In these samples, H0 is the time point just before hCG injection, H3 is the point when the EP2 receptor as well as COX-2 is induced in cumulus cells [22] and H9 is the time point when cumulus expansion occurs just before ovulation. H14 is the time point when the ovulated COCs are ready for fertilization after transition to the oviductal ampulla (see Fig. 1C). The cumulus cells were prepared by removing the oocytes from the COCs and they were then subjected to RNA extraction. The RNA obtained from cells at each time point was amplified, labeled and hybridized to microarrays.

Of the ~12,000 genes represented on the oligonucleotide array, genes in which the maximum minus minimum values between H0 and any of the time points were greater than 2 (a 2-fold change) were selected, and regarded as differentially expressed genes (3184 genes). Using the *k*-means clustering algorithm, these genes were classified into nine clusters (CLs) on the basis of similarity in their expression profiles (Fig. 1A). Among them, 2471 genes (77.6%) were up-regulated at least one time point compared with H0 (CLs 1–7), indicating that the main action of gonadotropin on cumulus cells is the induction of numerous genes. Of these up-regulated genes, 1865 genes (CLs 1–5) were induced immediately after gonadotropin injection (at least at H3) and the others (606 genes; CLs 6–7) were induced later at H14.

CLs 1–3 consist of genes in which expression levels were up-regulated only at H3 and then decreased, and CL4 consists of genes in which expression levels were up-regulated both at H3 and H9 and then decreased: CLs 1–4 comprise the gene group showing 'Early Transient' induction (Early Transient group in Fig. 1B–D and Table 1). CL5 consists of genes in which expression levels were up-regulated at H3 and sustained until H14: this CL is the gene group showing 'Early Sustained' induction (Early Sustained group in Fig. 1B–D and Table 1). In contrast, CLs 6–7 consist of genes in which expression levels were low both at H3 and H9 but up-regulated at H14: CLs 6–7 are therefore the gene group showing 'Late' induction (Late group in Fig. 1B–D and Table 2). Since there is no overlap between the genes of the 'Early' group and the 'Late' group, the functions of cumulus cells at H3 and H14 appear to be quite different. While CL8 consists of genes in which expression levels were down-regulated at H3 and then gradually recovered, CL9 consists of genes in which expression levels were constant at H3 but down-regulated at H9 and H14. CLs 8–9 (713 genes) comprise the gene group showing down-regulation upon gonadotropin stimulation (Down group in Fig. 1B, C and Table 3).

Since the microarray results were derived from a single array for each time point, they may contain 'false positive' genes. To evaluate the results, we selected genes representative for CL1 to CL9, and measured the expression levels of these genes by real-time RT-PCR using RNA from the independently isolated cumulus cells (Fig. 2). We chose *Piga* (CL1), *Bex1* (CL2), *Crem* (CL3), *Star* (CL4) from the 'Early transient' group, and these genes showed transient induction with a peak level at H3. *Acsl4* was selected from the 'Early sustained' group (CL5), which was actually induced at H3 and its expression level was kept at high levels until H14. *Mbp* (CL6) and *Cyp1b1* (CL7) were chosen from the 'Late' group, and their expression levels were induced at later stages. *Akap8* (CL8) and *Ccdn2* (CL9) were chosen from the 'Down-regulated' group, and the expression levels of *Akap8* and *Ccdn2* were immediately or gradually decreased, respectively. These results suggest that the microarray results are likely to be

Table 3
Genes down-regulated upon gonadotropin stimulation. The list represents genes in which expression levels were down-regulated at H3 and then gradually recovered (CL8) and genes in which expression levels were constant at H3 but down-regulated at H9 and H14 (CL9). The change in the expression level of each gene at each time point is indicated as a logarithm of the fold-change versus the expression level at H0, and the difference in the expression level of each gene in the cells at H3 (Early) or H14 (Late) versus at H0 are shown as a logarithm of the fold-change in bold. Representative genes with the largest changes are shown. ID, Affymetrix ID number.

Symbol	CL	Gene title	H3/H0 log2(fold)	H9/H0 log2(fold)	H14/H0 log2(fold)	ID
Early						
Vim	8	vimentin	**−2.2**	−0.8	−0.8	162379_r_at
Akap8	8	A kinase (PRKA) anchor protein 8	**−1.7**	−1.0	−0.9	161596_f_at
Nr5a1	8	nuclear receptor subfamily 5 group A member 1(SF1)	**−1.7**	−0.7	−0.9	161418_r_at
Eif4e	8	eukaryotic translation initiation factor 4E	**−1.7**	−0.9	−0.4	162222_r_at
Snx17	8	sorting nexin 17	**−1.7**	−0.9	−0.7	161257_r_at
Irf6	8	interferon regulatory factor 6	**−1.6**	−0.7	−0.9	161699_i_at
Btk	8	Bruton agammaglobulinemia tyrosine kinase	**−1.5**	−0.8	−0.6	161971_r_at
Timp1	8	tissue inhibitor of metalloproteinase 1	**−1.5**	−0.6	−0.7	162107_r_at
Late						
Inhbb	9	inhibin beta-B	−1.5	−2.5	**−5.3**	160828_at
Hpgd	9	hydroxyprostaglandin dehydrogenase 15 (NAD)	−1.0	−2.5	**−3.0**	93351_at
Ccnd2	9	cyclin D2	0.5	−1.4	**−2.6**	97504_at
Esr2	9	estrogen receptor 2 (beta)	−0.2	−1.6	**−2.6**	96514_at
Cdc6	9	cell division cycle 6 homolog	−0.6	−1.7	**−2.4**	103821_at
Inhba	9	inhibin beta-A	0.6	−1.7	**−2.2**	100277_at
Ptgis	9	prostaglandin I2 (prostacyclin) synthase	0.0	−1.6	**−2.2**	104538_at
Cyp2s1	9	cytochrome P450 family 2 subfamily s polypeptide 1	−1.0	−1.9	**−2.1**	104550_at

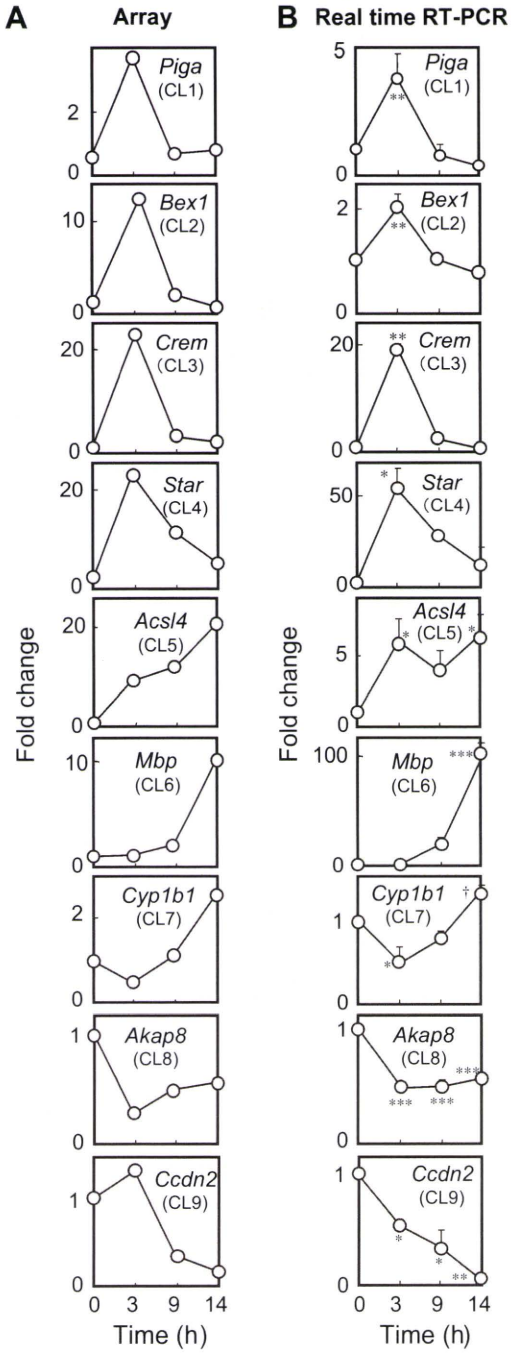

Fig. 2. Validation of the genes representative for each CL in WT cumuli. Temporal expression changes of genes representative for each CL in WT cumuli. The values represent the ratio of relative expression levels to H0. (A) Expression profiles obtained from oligonucleotide array analysis. (B) Expression profiles shown in (A) were verified by real-time RT-PCR. The values are shown as mean ± S.E.M. ($n = 4$–8). The specificity of the PCR product was confirmed by gel electrophoresis and analysis of the melting temperature. The expression level of each gene was normalized to *Gapdh*. *, $P < 0.05$; **, $P < 0.01$; ***, $P < 0.001$ (*vs* H0), †, $P < 0.05$ (*vs* H3).

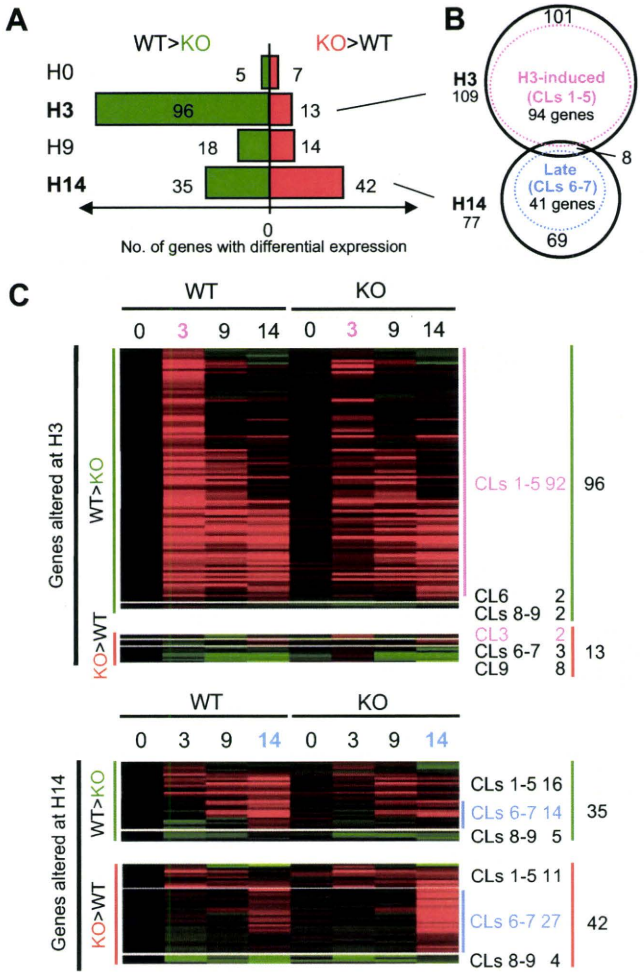

Fig. 3. *Ptger2* deficiency-sensitive genes. (A) The numbers of genes in which expression levels were altered by greater than 1.7-fold by *Ptger2* deficiency at H0, H3, H9 and H14. The number of genes in which expression levels were decreased (green) or increased in *Ptger2*$^{-/-}$ (KO) compared with WT cells (red) at each time point is shown to the left and right, respectively. (B) Genes are placed in groups corresponding to pairwise overlaps shown in the accompanying Venn diagrams. (C) Representation of genes in which expression levels were altered at H3 and H14 by *Ptger2* deficiency. Most of the genes sensitive to *Ptger2* deficiency at H3 belong to the H3-induced group (CLs 1–5), and more than half of the genes sensitive to *Ptger2* deficiency at H14 belong to the 'Late' induction group (CLs 6–7).

reliable in general, but careful evaluation using real-time RT-PCR is still recommended when discussing the detailed expression profiles of specific genes, especially with low hybridization signals.

The 'Early Transient' (CLs 1–4) and 'Early Sustained' (CL5) groups include many kinds of genes that are critical in several steps of preovulatory processes (Fig. 1D and Table 1). The induction of genes such as hyaluronan synthase 2 (*Has2*) and hyaluronan binding proteins (*Tnfaip6* and *Ptx3*) is necessary for the formation of the cumulus ECM [8–11,23]. Genes including PG-related genes such as *Ptgs2* and *Ptger4*, cAMP signaling-related genes such as *Crem*, *Nmu* and *Rgs10*, and epidermal growth factor (EGF) family genes such as *Areg*, *Ereg* and *Btc* have been suggested to initiate and amplify LH actions in oocyte maturation and cumulus expansion [18,24,25]. Induction of these genes was especially affected by *Ptger2* deficiency in cumulus cells as discussed below. Genes for other growth factors such as peroxisome proliferator activated receptor γ (*Pparg*), vascular endothelial growth factor A (*Vegfa*) and kit ligand (*Kitl*) have been indicated to be key mediators in ovulation and oocyte maturation [26–28].

In contrast, the 'Late' group (CLs 6–7) includes sets of genes that are quite different from those in the 'Early' groups as shown above (Fig. 1D and Table 2). There are two characteristic gene groups; one

Table 4
Genes down-regulated in *Ptger2*$^{-/-}$ cumulus cells at H3. The list represents genes in which expression levels were down-regulated by *Ptger2* deficiency at H3. The change in the expression level of each gene in WT cells at H3 versus in WT cells at H0 are indicated as a logarithm of the fold-change and the difference in the expression level of each gene in the *Ptger2*$^{-/-}$ cells (KO) versus in WT cells at H3 are shown as a logarithm of the fold-change in bold. Representative genes with the largest changes are shown. ID, Affymetrix ID number.

Symbol	CL	Gene title	WT (H3/H0) $\log_2$(fold)	H3 (KO/WT) $\log_2$(fold)	ID
Ptger2	3	prostaglandin E receptor 2 (subtype EP2)	1.0	**−1.7**	98768_at
Ifi202b	3	interferon activated gene 202B	3.1	**−1.7**	94774_at
Crem	3	cAMP responsive element modulator	4.7	**−1.6**	160526_s_at
Eil2	3	elongation factor RNA polymerase II 2	2.0	**−1.6**	103892_r_at
Procr	4	protein C receptor endothelial	5.5	**−1.6**	98018_at
Ptger4	3	prostaglandin E receptor 4 (subtype EP4)	2.5	**−1.4**	103362_at
Akr1b7	4	aldo–keto reductase family 1 member B7	3.0	**−1.4**	102826_at
Rgs10	3	regulator of G-protein signalling 10	2.2	**−1.3**	160629_at
Nmu	4	neuromedin	2.4	**−1.3**	161032_i_at
Efnb2	4	ephrin B2	1.5	**−1.3**	160857_at
Facl4	5	fatty acid–Coenzyme A ligase long chain 4	3.2	**−1.2**	104017_at
Star	4	steroidogenic acute regulatory protein	4.5	**−1.2**	92213_at
Areg	3	amphiregulin	6.6	**−1.2**	99915_at
Bex1	2	brain expressed gene 1	3.6	**−1.1**	93020_at
Bmp2k	3	BMP2 inducible kinase	1.6	**−1.1**	93376_at
Phlda1	4	pleckstrin homology-like domain family A 1	2.4	**−1.1**	160829_at
Cdkn1a	3	cyclin-dependent kinase inhibitor 1A (P21)	1.8	**−1.1**	98067_at
Ereg	4	epiregulin	3.0	**−0.9**	98802_at
Ptgs2	5	prostaglandin endoperoxide synthase 2	7.4	**−0.9**	104647_at
Akap2	3	A kinase (PRKA) anchor protein 2	1.1	**−0.8**	101435_at
Btc	4	betacellulin	2.7	**−0.6**	95310_at

includes ECM-related genes distinct from those found in the 'Early' group, such as procollagen family molecules (*Col4a1*, *Col18a1*, *Col4a2*, *Col6a1*), fibronectin 1 (*Fn1*), annexin A1 (*Anxa2*), integrin β1 (*Itgb1*) and matrix metalloproteinases (*Mmp11*, *Mmp14*, *Timp3*). Since changes in the ECM components surrounding the COCs in the oviduct have been shown to affect fertilization efficiency [29,30], the ECM components newly synthesized after ovulation may contribute to successful fertilization. The other gene group includes immune response-related genes, such as *Il10rb*, *Il13ra1* and chemokine-related genes. Induction of immune response-related genes may reflect adaptation of cumulus cells against the intraoviductal environment and their acquisition of self-protecting ability after ovulation [18].

The 'Down' group (CLs 8–9) can be subdivided into the 'Early down-regulated' group (CL8) and the 'Lately down-regulated' group (CL9). Each group includes several key genes (Fig. 1D and Table 3). The 'Early down-regulated' group (CL8) includes genes that are in the same functional category as seen in the 'Early Transient' group (CLs 1–4), but showed opposite behaviors. For instance, some cAMP-related genes, such as *Akap8* and *Irf6* were down-regulated. The 'Late down-regulated' group (CL9) includes the gene for hydroxyprostaglandin dehydrogenase (*hpgd*), an enzyme responsible for the catabolic breakdown of PGE_2.

3.2. Effect of Ptger2 deficiency on gene expression profiles in cumulus cells

To investigate the molecular basis of impaired cumulus cell function in *Ptger2*$^{-/-}$ mice, we performed similar analysis on cumulus cells isolated from *Ptger2*$^{-/-}$ mice and examined the effect of *Ptger2* deficiency. After time-matched comparison of expression signals between WT and *Ptger2*$^{-/-}$ cumuli, the genes demonstrating differential expression values of greater than 1.7

Table 5
Genes altered in *Ptger2*$^{-/-}$ cumulus cells at H14. The list represents genes in which expression levels were affected by *Ptger2* deficiency at H14. The change in expression level of each gene in WT cells at H14 versus in WT cells at H0 is indicated as a logarithm of the fold-change and the difference in the expression level of each gene in the *Ptger2*$^{-/-}$ (KO) cells versus in WT cells at H14 is shown as a logarithm of the fold-change in bold. Representative genes with the largest changes are shown. ID, Affymetrix ID number.

Symbol	CL	Gene title	WT (H14/H0) $\log_2$(fold)	H14 (KO/WT) $\log_2$(fold)	ID
Down-regulated in Ptger2$^{-/-}$					
Bnip3	7	BCL2/adenovirus E1B 19 kDa-interacting protein 1 NIP3	1.2	**−1.2**	93836_at
Atf2	5	activating transcription factor 2	1.4	**−1.1**	162010_r_at
Scd1	6	stearoyl-Coenzyme A desaturase 1	3.4	**−1.0**	94057_g_at
Mbp	6	myelin basic protein	3.3	**−0.9**	96311_at
Numb	6	numb gene homolog (Drosophila)	1.2	**−0.9**	161912_r_at
Cyp1b1	7	cytochrome P450 family 1 subfamily b polypeptide 1	1.4	**−0.9**	99979_at
Sparc	6	secreted acidic cysteine rich glycoprotein	3.0	**−0.8**	97160_at
Col18a1	6	procollagen type XVIII alpha 1	3.1	**−0.8**	101881_g_at
Cdh5	6	cadherin 5	1.9	**−0.8**	104083_at
Up-regulated in Ptger2$^{-/-}$					
Ccl2	6	chemokine (C–C motif) ligand 2 (MCP-1)	0.7	**2.0**	102736_at
Cxcl1	5	chemokine (C–X–C motif) ligand 1 (Groα)	1.0	**1.8**	95349_g_at
Gp49a	6	glycoprotein 49 A	2.6	**1.6**	100325_at
Ccr5	6	chemokine (C–C motif) receptor 5	1.1	**1.5**	161968_f_at
Anxa1	6	annexin A1	1.5	**1.3**	93037_i_at
C1qb	6	complement component 1 q subcomponent beta	0.5	**1.0**	96020_at
Ccl7	7	chemokine (C–C motif) ligand 7 (MCP-3)	−0.1	**1.0**	94761_at
Cxcl2	7	chemokine (C–X–C motif) ligand 2 (Groβ)	0.8	**0.9**	101160_at
Ccl9	7	chemokine (C–C motif) ligand 9 (MIP-1γ)	0.8	**0.9**	104388_at
Ccr2	7	chemokine (C–C) receptor 2	0.1	**0.8**	93397_at

(more than 1.7-fold increase or 1.7-fold decrease) in *Ptger2*$^{-/-}$ cumuli compared with WT were selected. The numbers of the selected genes at H0, H3, H9 and H14 were 12, 109, 32 and 77, respectively (Fig. 3A), indicating that *Ptger2* deficiency mainly affects cumulus cell transcription at H3 (ovulation) and H14 (fertilization). There were only a few overlaps (8 genes) between the H3 and H14 gene groups. Of the 109 genes with altered expression at H3, 96 genes were down-regulated in *Ptger2*$^{-/-}$ cumulus cells compared with WT cells (Fig. 3). Most of the genes with reduced expression (94 genes) belong to the 'H3-induced' CLs 1–5 (Fig. 3B and Table 4). On the other hand, of the 77 genes with altered expression at H14, 41 genes (53%) belong to the 'Late' induction group, and 42 and 35 genes were up- and down-regulated, respectively, upon *Ptger2* deficiency (Fig. 3, A and B, and Table 5).

To validate the results obtained by the single array analysis, we selected several genes with differential expression between WT and *Ptger2*$^{-/-}$ cells, and investigated the expression levels of these genes by real-time RT-PCR (Fig. 4). *Bex1* (CL2), and *Procr* (CL4) showed lower expression in *Ptger2*$^{-/-}$ cumuli at H3, and the expression levels of *Cyp1b1* (CL7) and *Mbp* (CL6) at H14 were attenuated in *Ptger2*$^{-/-}$ cumuli. In contrast, *C1qb* (CL6) and *Ccl2* (CL6) showed higher expression in *Ptger2*$^{-/-}$ cells at H14. Thus, the array results provide good candidates to screen genes regulated by PGE_2-EP2 signaling in the cumulus cells. Indeed, based on these array results, we identified chemokine-related genes, which play roles in maintenance of the cumulus ECM [14,15], as described below.

The genes down-regulated in *Ptger2*$^{-/-}$ cells include cAMP-related genes such as *Crem*; PG-related genes such as *Ptgs2* and *Ptger4*; and EGF family genes such as *Areg*, *Ereg* and *Btc*. We selected six genes, *Crem*, *Ptgs2*, *Ptger4*, *Areg*, *Ereg* and *Btc*, which have been shown to play key roles in cumulus cells, and examined the time course of their expression patterns by real-time RT-PCR (Fig. 5). In addition to the cumulus cells from the COCs, we isolated mural granulosa cells from the ovary, and examined whether *Ptger2* deficiency alters the expression of these genes specifically in the cumulus cells. As the array results indicated, the expression levels of the selected genes in the cumuli at H3 were significantly decreased in *Ptger2*$^{-/-}$ mice compared with WT, while there were no significant changes in the expression levels of these genes in mural granulosa cells between the two genotypes (Fig. 5, B and C). The fact that *Crem* and *Ptgs2* expression in the cumulus cells is attenuated by *Ptger2* deficiency suggests that PGE_2-EP2-cAMP signaling enhances *Ptgs2* expression (and presumably PGE_2 production) as a positive feed-back loop. Moreover, EP2 signaling appears to augment gene expression of the other cAMP-coupled PGE receptor, EP4.

Table 6
Primer sequences used for real time RT-PCR.

Gene	Forward	Reverse
Acsl4	5′-ggagggaatgtccgca-3′	5′-ctctggggttcggctt-3′
Akap8	5′-ccgacaactcagactcgc-3′	5′-ggagttgctccggtctt-3′
Areg	5′-agtcagagttgaacaggt-3′	5′-cctccaggttctcgat-3′
Bex1	5′-cgccatccctaacggag-3′	5′-cgccttgatctttggact-3′
Btc	5′-gaaaccaatggctctctt-3′	5′-cagacgccgatgacta-3′
C1qb	5′-aaggttcttcctgcctctag-3′	5′-cactgtgtcttcatcagctc-3′
Ccdn2	5′-cgccgtcgatgattgc-3′	5′-tgacgaacacgcctct-3′
Ccl2	5′-tgcaggtccctgtcatgcttc-3′	5′-cacagagagggaaaaatggatccacacc-3′
Crem	5′-ccttgccccaagtcacatg-3′	5′-agcagtagtaggagctcggatctg-3′
Cyp1b1	5′-ctaggtctcggggtcc-3′	5′-aggcgagcgaagtaca-3′
Ereg	5′-cacaaccgtgatccca-3′	5′-gtcaacgcaacgtattct-3′
Gapdh	5′-tgaacgggaagctcactgg-3′	5′-tccaccaccctgttgctgta-3′
Mbp	5′-gactcacacacgagaactac-3′	5′-tcgaggtgtcacaatgttct-3′
Piga	5′-ggttggtgggattcccg-3′	5′-ttccttcgacactcgct-3′
Procr	5′-gcgcaaggagaacgtg-3′	5′-ataccgagtccggttgt-3′
Ptger4	5′-ttccgctcgtggtgcgagtgttc-3′	5′-gaggtggtgtctgcttgggtcag-3′
Ptgs2	5′-agtgtgcgacatactca-3′	5′-gcgtttgcggtactca-3′
Star	5′-cgtgcgctgtaccaag-3′	5′-tctgggtctgcgatagg-3′

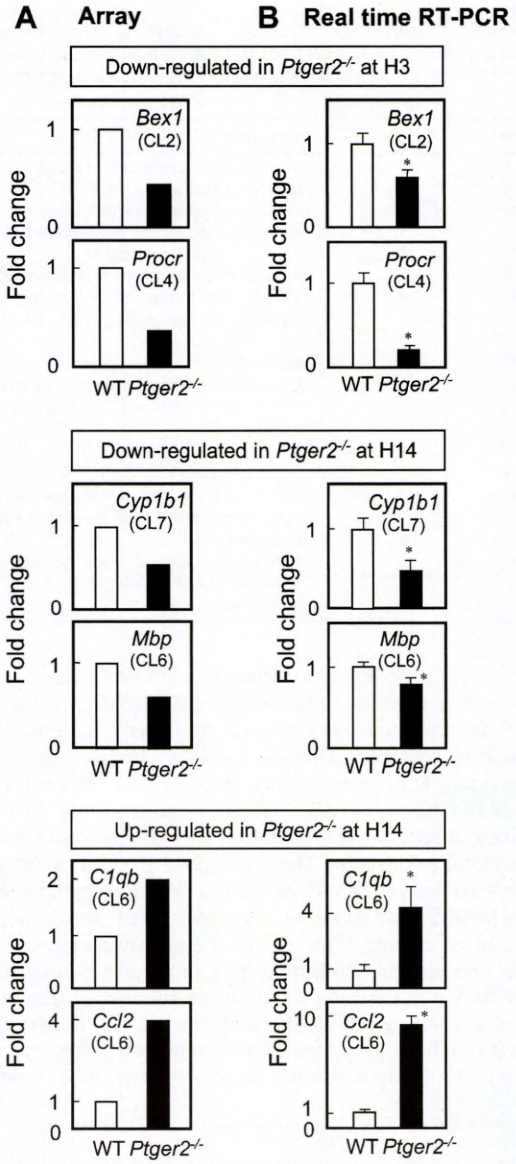

Fig. 4. Validation of the genes differentially expressed between WT and *Ptger2*$^{-/-}$ cumuli. Representative genes in which their expression levels were down-regulated at H3 (*Bex1*, *Procr*) or at H14 (*Cyp1b1*, *Mbp*), or up-regulated at H14 upon *Ptger2* deficiency (*C1qb*, *Ccl2*). The values represent the ratio of relative expression levels to WT cumulus cells. (A) Expression levels obtained from oligonucleotide array analysis. (B) Expression profiles shown in (A) were verified by real-time RT-PCR. The values are shown as mean ± S.E.M. (n = 4–8). The specificity of the PCR product was confirmed by gel electrophoresis and analysis of the melting temperature. The expression level of each gene was normalized to *Gapdh*. *, $P < 0.05$ (*vs* WT).

Since cumulus cells have been shown to express the LH receptor at minimal levels in mice [31], and since the expression levels of *Crem* were significantly attenuated, the EP2 receptor appears to play a pivotal role in cAMP signaling in cumulus cells under physiological conditions. Therefore, attenuated expression levels of cAMP-driven genes may cause the defective ovulation observed in *Ptger2*$^{-/-}$ mice. Indeed, the expression of EGF family genes was attenuated by *Ptger2* deficiency. These genes are clustered in a region of mouse chromosome 5 [32] and are induced by LH-cAMP signaling both in mural and cumulus cells [18,25]. These EGF-like growth factors stimulate cumulus expansion and oocyte maturation via tyrosine kinase-type EGF receptor signaling in cumulus cells. Indeed, based on the

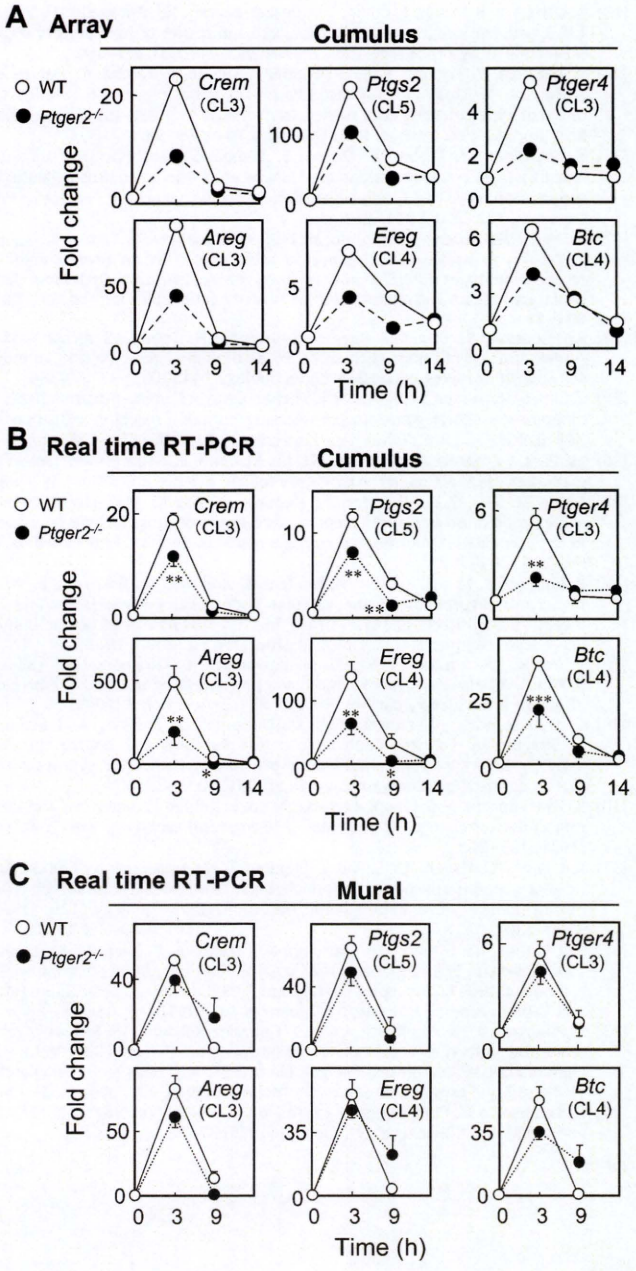

Fig. 5. *Ptger2* deficiency attenuates expression levels of *Crem*, *Ptgs2*, *Ptger4*, *Areg*, *Ereg* and *Btc* in a cumulus-specific manner at H3. Time course of *Crem*, *Ptgs2*, *Ptger4*, *Areg*, *Ereg* and *Btc* gene expression in WT and *Ptger2*$^{-/-}$ cumulus and mural granulosa cells. (A) Time course of expression profiles in cumulus cells by oligonucleotide array analysis. (B and C) Cumulus cells (B) or mural granulosa cells (C) were isolated from WT and *Ptger2*$^{-/-}$ mice at the indicated time points after hCG injection, and their RNA was extracted and subjected to real time-RT PCR. The values are shown as mean ± S.E.M. (n = 4–8). The specificity of the PCR product was confirmed by gel electrophoresis and analysis of the melting temperature. The expression level of each gene was normalized to *Gapdh*. **, $P < 0.01$; ***, $P < 0.001$ (*vs* WT).

alterations of gene expression profiles of COCs upon *Ptgs2* deficiency, Shimada et al. previously proposed the possibility that PG signaling potentiates gene expression of EGF-like growth factors [33]. Thus, the EP2 receptor likely induces not only cAMP signaling but also EGF receptor signaling in the cumulus cells, and such appropriate signaling cascades in the cumulus cells are thought to be required for successful ovulation.

As we recently reported [14], one of the most remarkable changes in the *Ptger2*$^{-/-}$ cumulus at H14 is the increased expression of chemokine-related genes including *Ccl2*, *Ccl7*, *Ccl9*, *Cxcl1*, *Cxcl2*, *Ccr2* and *Ccr5* (Table 5). We further demonstrated that enhanced CCL signaling in the cumulus elicits excessive integrin engagement to the cumulus ECM through Rho/ROCK/actomyosin pathway [15]. It is interesting in this respect that other sets of ECM-related genes including myelin basic protein (*Mbp*) and secreted acidic cysteine-rich glycoprotein (*Sparc*) were down-regulated while CCL signaling alters the cumulus ECM status. Whether the expression of these ECM-related genes and cumulus ECM status are regulated by the balance between EP2 and chemokine signaling is an interesting issue to be examined.

The results obtained in this study, especially the temporal changes in gene expression profiles of WT cumulus cells generally showed excellent agreement with the previous report by Hernandez-Gonzalez et al., in which gene expression profiles of COCs were examined [18]. For example, they reported that; (1) expression levels of EGF-like growth factors are induced by hCG injection, (2) neuron-related genes such as *Mbp* and *Tnc*, and immune cell-related genes such as *Alcam* are induced after ovulation, and (3) the expression of cell cycle-related genes such as *Ccnd2* is gradually decreased. These tendencies were reproduced in the current study, suggesting that such results may reflect the gene expression profiles of cumulus cells. In contrast, oocyte-specific genes such as *Zp1* were not included in this study. On the other hand, we detected a transient but significant induction of the *Crem* gene, a transcription factor for cAMP-driven gene expression [34], which has never been reported in previous studies using COCs as a target. Thus, gene expression analysis of identical types of cells is useful for assessing second messenger-based signaling cascades.

In summary, we clarified the temporal changes in cumulus gene expression profiles of WT mice and the effect of *Ptger2* deficiency on them. These results indicate that the gene expression profile of cumulus cells greatly differs before and after ovulation, and in each situation, PGE_2-EP2 signaling plays a critical role in cAMP-regulated gene expression in the cumulus cells under physiological conditions. Results from the present study will be useful not only for understanding the role of PGE_2 in ovulation and fertilization but also for discovering new insights into the functions of the cumulus and ECM in ovulation and fertilization.

Acknowledgements

S.T. was supported by a research fellowship from the Japan Society for the Promotion of Science for Young Scientists. This work was supported in part by Grants-in-Aid for Scientific Research and on Priority Areas 'Applied Genomics' and 'Mechanisms of Sex Differentiation' from the Ministry of Education, Culture, Sports, Science, and Technology of Japan, from the Ministry of Health and Labor of Japan, from the National Institute of Biomedical Innovation of Japan, from the Mochida Memorial Foundation and the Naito Foundation. We thank K. Nakayama and S. Tsuchiya for their continuous support. We also thank Y. Hirose, M. Hirose, and Y. Noda for their technical support and helpful advice. We are also grateful to H.A. Popiel and Y. Nakaminami for careful reading of the manuscript and secretary assistance, respectively.

References

[1] A. Trafriri, S.Y. Chun, Ovulation. in: E.Y. Adashi, J.A. Rosenwaks (Eds.), Reproductive Endocrinology, Surgery, and Technology. Lippincot, Philadelphia, 1996, pp. 235–249.
[2] P.M. Wassarman, The mammalian ovum. in: E. Knobil, J.D. Neil (Eds.), The Physiology of Reproduction. Raven, New York, 1994, pp. 79–122.

[3] J.S. Richards, D.L. Russell, S. Ochsner, L.L. Espey, Ovulation: new dimensions and new regulators of the inflammatory-like response. Annu. Rev. Physiol. 64 (2002) 69–92.
[4] M.M. Matzuk, K.H. Burns, M.M. Viveiros, J.J. Eppig, Intercellular communication in the mammalian ovary: oocytes carry the conversation. Science 296 (2002) 2178–2180.
[5] P. Talbot, B.D. Shur, D.G. Myles, Cell adhesion and fertilization: steps in oocyte transport, sperm-zona pellucida interactions, and sperm–egg fusion. Biol. Reprod. 68 (2003) 1–9.
[6] S. Tanghe, A. Van Soom, H. Nauwynck, M. Coryn, A. de Kruif, Minireview: functions of the cumulus oophorus during oocyte maturation, ovulation, and fertilization. Mol. Reprod. Dev. 61 (2002) 414–424.
[7] P. Primakoff, D.G. Myles, Penetration, adhesion, and fusion in mammalian sperm–egg interaction. Science 296 (2002) 2183–2185.
[8] A. Salustri, C. Garlanda, E. Hirsch, M. De Acetis, A. Maccagno, B. Bottazzi, A. Doni, A. Bastone, G. Mantovani, P. Beck Peccoz, G. Salvatori, D.J. Mahoney, A. J. Day, G. Siracusa, L. Romani, A. Mantovani, PTX3 plays a key role in the organization of the cumulus oophorus extracellular matrix and in in vivo fertilization. Development 131 (2004) 1577–1586.
[9] L. Zhuo, M. Yoneda, M. Zhao, W. Yingsung, N. Yoshida, Y. Kitagawa, K. Kawamura, T. Suzuki, K. Kimata, Defect in SHAP-hyaluronan complex causes severe female infertility. A study by inactivation of the bikunin gene in mice. J. Biol. Chem. 276 (2001) 7693–7696.
[10] S. Varani, J.A. Elvin, C. Yan, J. DeMayo, F.J. DeMayo, H.F. Horton, M.C. Byrne, M.M. Matzuk, Knockout of pentraxin 3, a downstream target of growth differentiation factor-9, causes female subfertility. Mol. Endocrinol. 16 (2002) 1154–1167.
[11] C. Fulop, S. Szanto, D. Mukhopadhyay, T. Bardos, R.V. Kamath, M.S. Rugg, A.J. Day, A. Salustri, V.C. Hascall, T.T. Glant, K. Mikecz, Impaired cumulus mucification and female sterility in tumor necrosis factor-induced protein-6 deficient mice. Development 130 (2003) 2253–2261.
[12] H. Lim, B.C. Paria, S.K. Das, J.E. Dinchuk, R. Langenbach, J.M. Trzaskos, S.K. Dey, Multiple female reproductive failures in cyclooxygenase 2-deficient mice. Cell 91 (1997) 197–208.
[13] H. Hizaki, E. Segi, Y. Sugimoto, M. Hirose, T. Saji, F. Ushikubi, T. Matsuoka, Y. Noda, T. Tanaka, N. Yoshida, S. Narumiya, A. Ichikawa, Abortive expansion of the cumulus and impaired fertility in mice lacking the prostaglandin E receptor subtype EP_2. Proc. Natl. Acad. Sci. USA 96 (1999) 10501–10506.
[14] S. Tamba, R. Yodoi, E. Segi-Nishida, A. Ichikawa, S. Narumiya, Y. Sugimoto, Timely interaction between prostaglandin and chemokine signaling is a prerequisite for successful fertilization. Proc. Natl. Acad. Sci. USA 105 (2008) 14539–14544.
[15] R. Yodoi, S. Tamba, K. Morimoto, E. Segi-Nishida, M. Nishihara, A. Ichikawa, S. Narumiya, Y. Sugimoto, RhoA/Rho kinase signaling in the cumulus mediates extracellular matrix assembly. Endocrinology 150 (2009) 3345–3352.
[16] L.L. Espey, J.S. Richards, Temporal and spatial patterns of ovarian gene transcription following an ovulatory dose of gonadotropin in the rat. Biol. Reprod. 67 (2002) 1662–1670.
[17] M. Jo, M.C. Gieske, C.E. Payne, S.E. Wheeler-Price, J.B. Gieske, I.V. Ignatius, T.E. Curry Jr., C. Ko, Development and application of a rat ovarian gene expression database. Endocrinology 145 (2004) 5384–5396.
[18] I. Hernandez-Gonzalez, I. Gonzalez-Robayna, M. Shimada, C.M. Wayne, S.A. Ochsner, L. White, J.S. Richards, Gene expression profiles of cumulus cell oocyte complexes during ovulation reveal cumulus cells express neuronal and immune-related genes: does this expand their role in the ovulation process? Mol. Endocrinol. 20 (2006) 1300–1321.
[19] R.A. Irizarry, B. Hobbs, F. Collin, Y.D. Beazer-Barclay, K.J. Antonellis, U. Scherf, T.P. Speed, Exploration, normalization, and summaries of high density oligonucleotide array probe level data. Biostatistics 4 (2003) 249–264.
[20] S. Tsuchiya, Y. Tachida, E. Segi-Nishida, Y. Okuno, S. Tamba, G. Tsujimoto, S. Tanaka, Y. Sugimoto, Characterization of gene expression profiles for different types of mast cells pooled from mouse stomach subregions by an RNA amplification method. BMC Genomics 10 (2009) 35.
[21] Y. Sugimoto, H. Tsuboi, Y. Okuno, S. Tamba, S. Tsuchiya, G. Tsujimoto, A. Ichikawa, Microarray evaluation of EP4 receptor-mediated prostaglandin E_2 suppression of 3T3-L1 adipocyte differentiation. Biochem. Biophys. Res. Commun. 322 (2004) 911–917.
[22] E. Segi, K. Haraguchi, Y. Sugimoto, M. Tsuji, H. Tsunekawa, S. Tamba, K. Tsuboi, S. Tanaka, A. Ichikawa, Expression of messenger RNA for prostaglandin E receptor subtypes EP4/EP2 and cyclooxygenase isozymes in mouse periovulatory follicles and oviducts during superovulation. Biol. Reprod. 68 (2003) 804–811.
[23] S.A. Ochsner, A.J. Day, M.S. Rugg, R.M. Breyer, R.H. Gomer, J.S. Richards, Disrupted function of tumor necrosis factor-α-stimulated gene 6 blocks cumulus cell–oocyte complex expansion. Endocrinology 144 (2003) 4376–4384.
[24] C. Castro-Fernandez, S.P. Brothers, P. Michael Conn, A Galphas mutation (D229S) differentially effects gonadotropin-releasing hormone receptor regulation by RGS10, RGS3 and RGS3T. Mol. Cell. Endocrinol. 200 (2003) 119–126.
[25] J.Y. Park, Y.Q. Su, M. Ariga, E. Law, S.L. Jin, M. Conti, EGF-like growth factors as mediators of LH action in the ovulatory follicle. Science 303 (2004) 682–684.
[26] J. Kim, M. Sato, Q. Li, J.P. Lydon, F.J. Demayo, I.C. Bagchi, M.K. Bagchi, Peroxisome proliferator-activated receptor γ is a target of progesterone regulation in the preovulatory follicles and controls ovulation in mice. Mol. Cell. Biol. 28 (2008) 1770–1782.
[27] R. Einspanier, M. Schönfelder, K. Müller, M. Stojkovic, M. Kosmann, E. Wolf, D. Schams, Expression of the vascular endothelial growth factor and its receptors and effects of VEGF during in vitro maturation of bovine cumulus–oocyte complexes (COC). Mol. Reprod. Dev. 62 (2002) 29–36.
[28] Y. Ye, K. Kawamura, M. Sasaki, N. Kawamura, P. Groenen, M.D. Gelpke, R. Rauch, A.J. Hsueh, T. Tanaka, Kit ligand promotes first polar body extrusion of mouse preovulatory oocytes. Reprod. Biol. Endocrinol. 7 (2009) 26.
[29] C. D'Alessandris, R. Canipari, M. Di Giacomo, O. Epifano, A. Camaioni, G. Siracusa, A. Salustri, Control of mouse cumulus cell–oocyte complex integrity before and after ovulation: plasminogen activator synthesis and matrix degradation. Endocrinology 142 (2001) 3033–3040.
[30] R. Yanagimachi, M.C. Chang, Fertilizable life of golden hamster ova and their morphological changes at the time of losing fertilizability. J. Exp. Zool. 148 (1961) 185–203.
[31] X.R. Peng, A.J. Hsueh, P.S. LaPolt, L. Bjersing, T. Ny, Localization of luteinizing hormone receptor messenger ribonucleic acid expression in ovarian cell types during follicle development and ovulation. Endocrinology 129 (1991) 3200–3207.
[32] B.G. Pathak, D.J. Gilbert, C.A. Harrison, N.C. Luetteke, X. Chen, M. Klagsbrun, G.D. Plowman, N.G. Copeland, N.A. Jenkins, D.C. Lee, Mouse chromosomal location of three EGF receptor ligands: amphiregulin (Areg), betacellulin (Btc), and heparin-binding EGF (Hegfl). Genomics 28 (1995) 116–118.
[33] M. Shimada, I. Hernandez-Gonzalez, I. Gonzalez-Robayna, J.S. Richards, Paracrine and autocrine regulation of epidermal growth factor-like factors in cumulus oocyte complexes and granulosa cells: key roles for prostaglandin synthase 2 and progesterone receptor. Mol. Endocrinol. 20 (2006) 1352–1365.
[34] P. Sassone-Corsi, Coupling gene expression to cAMP signalling: role of CREB and CREM. Int. J. Biochem. Cell Biol. 30 (1998) 27–38.

Bioorganic & Medicinal Chemistry Letters 20 (2010) 2350–2353

Contents lists available at ScienceDirect

Bioorganic & Medicinal Chemistry Letters

journal homepage: www.elsevier.com/locate/bmcl

A reverse transcriptase stop assay revealed diverse quadruplex formations in UTRs in mRNA

Masaki Hagihara [a], Keisuke Yoneda [a], Hiroaki Yabuuchi [b], Yasushi Okuno [b], Kazuhiko Nakatani [a,*]

[a] Department of Regulatory Bioorganic Chemistry, The Institute of Scientific and Industrial Research (ISIR), Osaka University, Ibaraki 567-0047, Japan
[b] Department of Systems Bioscience for Drug Discovery, Graduate School of Pharmaceutical Sciences, Kyoto University, Kyoto 606-8501, Japan

ARTICLE INFO

Article history:
Received 30 November 2009
Revised 21 January 2010
Accepted 25 January 2010
Available online 17 February 2010

Keywords:
RNA quadruplex
Reverse transcriptase
mRNA

ABSTRACT

Here, we developed a reverse transcriptase based method (*RTase* stop assay) to characterize quadruplex formations in guanine-rich RNAs with high sensitivity and specificity. By using the *RTase* stop assay, we also revealed a plausible structural polymorphism in biologically important RNAs. The *RTase* stop assay would provide helpful insight into RNA quadruplex structures and functions, together with other analytical methods, including various footprinting techniques.

A wide variety of RNA plays an important role in the regulation of biological function within cells. The function of RNA largely depends on tertiary structures, in which RNA molecules use specific hydrogen bonds, including Watson–Crick and Hoogsteen bonds, to form active structures. Among a variety of RNA ternary folded structures, quadruplexes are one of the unique structures, in which guanine tetrads make Hoogsteen hydrogen bonds with each other in plane with incorporating metal ion, such as potassium and sodium, inside the tetrads.[1–3] Recent reports have demonstrated that quadruplex structures in untranslated regions (UTRs) in mRNAs are involved in the translational regulation in vitro and vivo.[4–6]

Computational predictions[7] together with various analytical methods, including spectroscopic methods[8,9] and footprinting techniques,[10–12] are commonly used to deduce secondary and tertiary structures of RNAs. Each technique has inherent advantages and disadvantages with regard to the quadruplex formations in RNAs, although spectroscopic analyses by using model oligonucleotides suggested that guanine-rich RNAs are easy to form quadruplex structures.[4–6,13] Simple and sensitive methods addressing RNA quadruplexes would provide deeper understandings of RNA quadruplex structures and functions.

Reverse transcriptases have been used to predict stable secondary structures in RNAs, involving quadruplex structures, however, the sensitivities of these assays are sometimes too low to fully address the sequence–structure relationships of quadruplex formation.[14,15] Here, we reported a reverse transcription based method to precisely evaluate the stability and the structural diversity of quadruplexes in RNAs.

In order to gain insight into local quadruplex structures on an RNA template, we studied an RNA-dependent DNA polymerase stop assay, named a reverse transcriptase stop assay (*RTase* stop assay) (Fig. 1A). In the *RTase* stop assay, reverse transcriptases, such as those originated from Moloney murine leukemia virus (M-MuLV), proceeded along RNA templates until the enzyme encountered stable RNA quadruplex structures. Interference of *RTase* reaction by quadruplex structures on the templates would result in the production of truncated complement DNA products, which can be detected by PAGE analyses.[16,17]

First, a human telomeric sequence 5′-r(UUAGGG)$_4$UUA-3′ (**R-telo27**) was chosen as a model of RNA quadruplexes.[13,18] **R-telo27** showed UV-melting curves with an inverse transition at 295 nm.[19] The melting temperature showed a significant KCl concentration-dependency (Fig. 1B) with T_m values of 61.7 ± 0.2 °C and 76.5 ± 0.3 °C in 10 and 100 mM KCl, respectively. CD spectra of **R-telo27** in the both KCl solutions suggested a parallel stranded quadruplex conformer, exhibiting a strong positive peak at 263 nm and a relatively weak peak near 240 nm (Fig. 1C). These data suggested that **R-telo27** having a four-telomeric-repeat afforded quadruplex structures with a different stability, depending on the KCl concentrations.

With the biophysical information of quadruplex stabilities in hand, we next investigated quadruplex formations by the *RTase* stop assay on RNA templates that contained the **R-telo27** sequence at the center of the template. In 100 mM KCl, the *RTase* reaction was exclusively interrupted at the first GGG site from 3′-end of the templates, where a plausible quadruplex was formed, regard-

* Corresponding author.
E-mail address: nakatani@sanken.osaka-u.ac.jp (K. Nakatani).

0960-894X/$ - see front matter © 2010 Elsevier Ltd. All rights reserved.
doi:10.1016/j.bmcl.2010.01.158

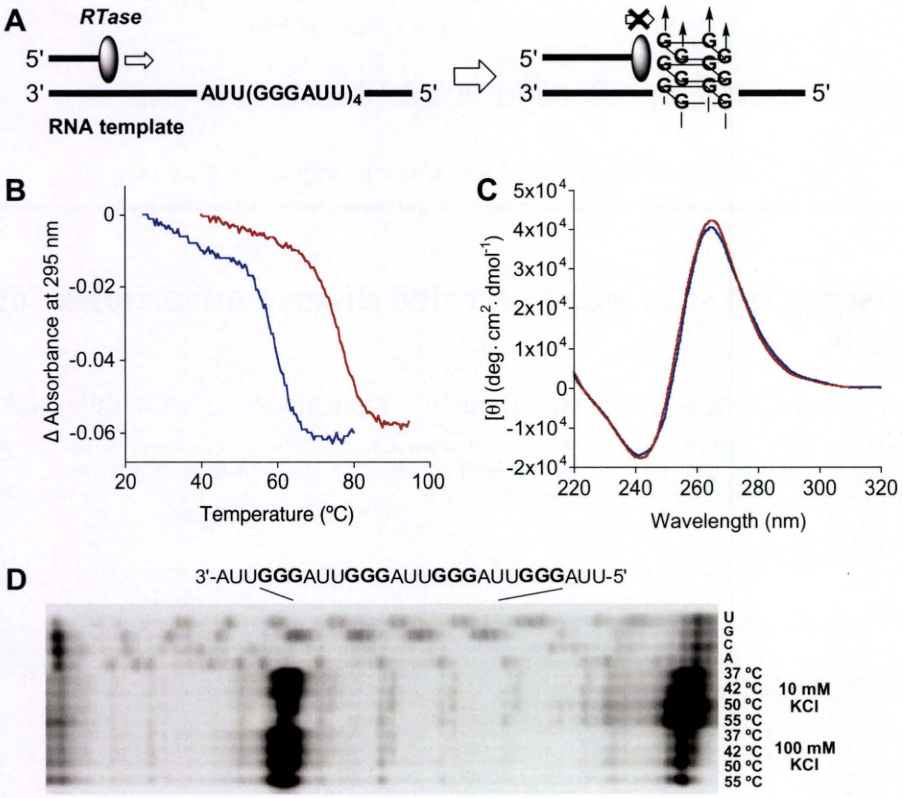

Figure 1. (A) Schematic illustration of a reverse transcriptase stop assay on a four-telomeric-repeat containing RNA. (B, C) Biophysical properties of a four-telomeric-repeat RNA (**R-telo27**). (B) T_m melting curves of **R-telo27** and (C) CD spectra of **R-telo27**. All experiments were carried out at 5 μM **R-telo27** in the 10 mM sodium cacodylate buffer (pH 7.0) containing 10 mM (blue) and 100 mM (red) KCl at 25 °C. (D) Interruption of *RTase*-mediated DNA synthesis with different reaction temperatures on RNA templates in the presence of KCl. The lane markers U, G, C, and A indicate the bases on the template strand. Guanines in the telomeric-repeat regions were emphasized in bold.

less of increasing temperatures from 37 to 55 °C (Fig. 1D). While, in 10 mM KCl, the paused products gradually decreased concomitant with increasing reaction temperature. These observations are well correlated with the decreased stability of quadruplex structure observed in the melting analysis. In contrast, no apparent paused bands were detected for *RTase* reaction on the RNA template containing a hairpin-loop structure (see Fig. S1 in Supplementary data), suggesting that the quadruplex structures serve as an effective inhibitor of *RTase* possibly due to their aberrant structures.

To certify the quadruplex formations in the four-telomeric-repeat RNA, a series of RNA variants (Table 1) was tested by the *RTase* stop assay. These variants had a deletion of a GGG sequence (*D*IV), single guanine mutations to adenine in each GGG sequence (mut I, II, III, and IV), or an insertion of the GGG upstream of the guanine-rich region of *D*IV (mut V) with an entire RNA length kept unchanged.

As shown in Figure 2, (1) the *RTase* reaction was not at all interfered on the RNA template containing a three-telomeric-repeat (*D*IV), (2) the variants containing even the single guanine-to-adenine mutations inside each GGG sequence did not show any paused products (mut I, II, III, and IV), and (3) the paused bands were clearly observed by the insertion of the GGG at the nine-base upstream of the position IV. The remarkable differences with regard to the number of repeats would attribute to capabilities of the quadruplex formations in the RNA templates. Considering that stable quadruplex formations generally require an association of four strands having at least three-guanine-repeat, the *RTase* stop assay would correctly provide information of an intrastranded RNA quadruplex formation. Also, these results suggested that RNA quadruplex structures were tolerant to the linker-length between GGG units, possibly due to a flexible feature of single-stranded RNAs. Taken together, the *RTase* stop assay revealed an intrinsic propensity for RNA quadruplex formations.

Next, we investigated the formation of quadruplex in UTRs by the *RTase* stop assay. Bioinformatic analysis suggested genetically conserved potential quadruplex structure sequences (PQSSs) both

Table 1
Telomeric RNA mutants used in this study

3′-	I		II		III		IV		V		-5′
AUU	**GGG**	AUU	**GGG**	AUU	**GGG**	AUU	**GGG**	AUU			Wild-type
AUU	**GGG**	AUU	**GGG**	AUU	**GGG**	AUU	**AAA**	AUU			ΔIV
AUU	**GGG**	AUU	**GGG**	AUU	**GGG**	AUU	**GAG**	AUU			mut IV
AUU	**GGG**	AUU	**GGG**	AUU	**GAG**	AUU	**GGG**	AUU			mut III
AUU	**GGG**	AUU	**GAG**	AUU	**GGG**	AUU	**GGG**	AUU			mut II
AUU	**GAG**	AUU	**GGG**	AUU	**GGG**	AUU	**GGG**	AUU			mut I
AUU	**GGG**	AUU	**GGG**	AUU	**GGG**	AUU	**AAA**	AUU	UCGCAU	**GGG**	mut V

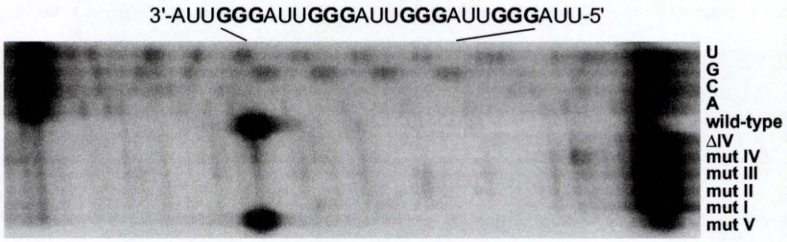

Figure 2. Quadruplex formations in the various telomeric-repeat mutants. The *RTase* reaction was performed at 42 °C in 100 mM KCl buffer. The lane markers U, G, C, and A indicate the bases on the template strand of the wild-type RNA. Guanines in the telomeric-repeat regions were emphasized in a bold case.

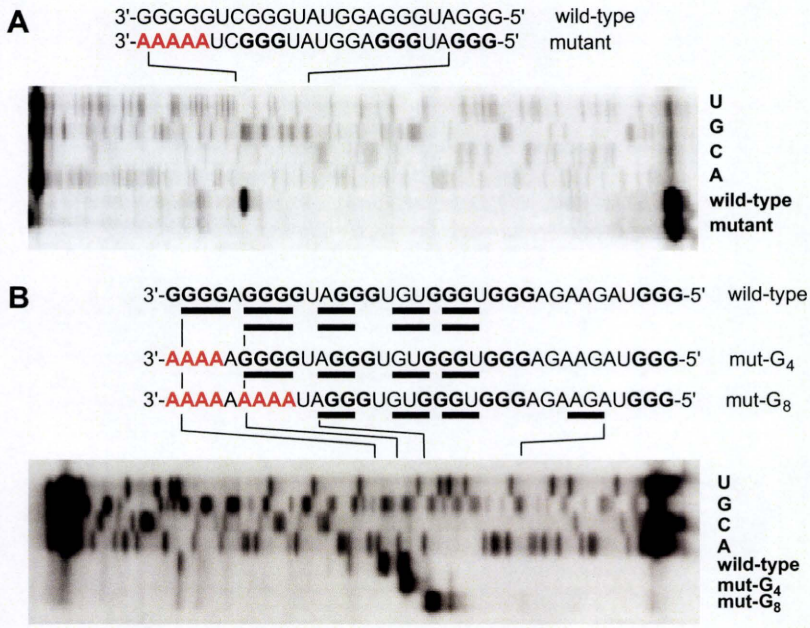

Figure 3. Quadruplex formations in the PQSS in 5′- and 3′-UTRs. Probing quadruplex formation (A) in the wild-type *GLI* 3′-UTR and its mutant and (B) in the *INHA* 5′-UTR. Bar indicated the PQSSs in the UTRs. The lane markers U, G, C, and A indicate the bases on the template strand of the wild-type UTRs.

in 5′- and 3′-UTRs. We focused on the two PQSSs in the human transcription factor Gli1 (*GLI*) 3′-UTR and in the inhibin-A (*INHA*) 5′-UTR. The *GLI* encoded a zinc finger protein that mediates Hedgehog signaling at the end of the pathway, and activation of Gli1 protein has been shown to be responsible for tumorigenesis.[20] The *INHA* encodes peptide hormone that inhibits the production of follicle-stimulating hormone (FSH) by the pituitary gland. The inhibins play roles in the control of gametogenesis, and embryonic and fetal development.[21]

The *GLI* 3′-UTR exclusively gave paused bands at the 3′-side of the PQSS (5′-**GGG**AU**GGG**AGGUAU**GGG**CU**GGGGG**-3′) (Fig. 3A). A GGGGG-to-AAAAA mutation (5′-**GGG**AU**GGG**AGGUAU**GGG**CU**AAAAA**-3′) in the PQSS completely disrupted the formation of quadruplex as observed in the wild-type *GLI* 3′-UTR. This observation suggested the stable quadruplex formation in the guanine-rich *GLI* PQSS.

While, the *INHA* 5′-UTR gave two major paused bands in the PQSS (5′-**GGG**UAGAAGA**GGG**U**GGG**UGU**GGG**AU**GGGGA**GGGG-3′) (Fig. 3B, lane 5). Sequential mutations of guanine-repeat units from the 3′-side of the PQSS moved the formation of paused products to 5′-side of the templates (Fig. 3B, lanes 6 and 7). Furthermore, all the paused products were assigned to be at the 3′-side of the guanine-repeat in the PQSS, implying that guanine-repeat regions can afford a variety of quadruplex formations in UTRs.

The *RTase* stop assay described here provided direct evidence for quadruplex formation in these UTRs, as well as information regarding the structural diversity of quadruplexes in the PQSS. The resolution of the *RTase* stop assay is high enough to address the structural diversity of quadruplexes, which would be feasible in many other guanine-rich regions in UTRs.

Acknowledgement

This work was supported by the Human Frontier Science Program Award HFSP RGY79/2007

Supplementary data

Supplementary data associated with this article can be found, in the online version, at doi:10.1016/j.bmcl.2010.01.158.

References and notes

1. Burge, S.; Parkinson, G. N.; Hazel, P.; Todd, A. K.; Neidle, S. *Nucleic Acids Res.* **2006**, *34*, 5402.
2. Patel, D. J.; Phan, A. T.; Kuryavyi, V. *Nucleic Acids Res.* **2007**, *35*, 7429.
3. Lane, A. N.; Chaires, J. B.; Gray, R. D.; Trent, J. O. *Nucleic Acids Res.* **2008**, *36*, 5482.

4. Kumari, S.; Bugaut, A.; Huppert, J. L.; Balasubramanian, S. *Nat. Chem. Biol.* **2007**, *3*, 218.
5. Arora, A.; Dutkiewicz, M.; Scaria, V.; Hariharan, M.; Maiti, S.; Kurreck, J. *RNA* **2008**, *14*, 1.
6. Wieland, M.; Hartig, J. S. *Chem. Biol.* **2007**, *14*, 757.
7. Zuker, M. *Nucleic Acids Res.* **2003**, *31*, 3406.
8. Scott, L. G.; Hennig, M. *Methods Mol. Biol.* **2008**, *452*, 29.
9. Golden, B. L. *Methods Mol. Biol.* **2007**, *363*, 239.
10. Ryder, S. P.; Ortoleva-Donnelly, L.; Kosek, A. B.; Strobel, S. A. *Methods Enzymol.* **2000**, *317*, 92.
11. Tullius, T. D.; Greenbaum, J. A. *Curr. Opin. Chem. Biol.* **2005**, *9*, 127.
12. Soukup, G. A.; Breaker, R. R. *RNA* **1999**, *5*, 1308.
13. Sacca, B.; Lacroix, L.; Mergny, J. L. *Nucleic Acids Res.* **2005**, *33*, 1182.
14. Nielsen, F. C.; Christiansen, J. *J. Biol. Chem.* **1992**, *267*, 19404.
15. Schaeffer, C.; Bardoni, B.; Mandel, J. L.; Ehresmann, B.; Ehresmann, C.; Moine, H. *EMBO J.* **2001**, *20*, 4803.
16. Han, H.; Hurley, L. H.; Salazar, M. *Nucleic Acids Res.* **1999**, *27*, 537.
17. Hagihara, M.; Goto, Y.; Nakatani, K. *ChemBioChem* **2008**, *9*, 510.
18. Xu, Y.; Kaminaga, K.; Komiyama, M. *J. Am. Chem. Soc.* **2008**, *130*, 11179.
19. Mergny, J. L.; Phan, A. T.; Lacroix, L. *FEBS Lett.* **1998**, *435*, 74.
20. Stecca, B.; Ruiz, I.; Altaba, A. *J. Neurobiol.* **2005**, *64*, 476.
21. Kitisin, K.; Saha, T.; Blake, T.; Golestaneh, N.; Deng, M.; Kim, C.; Tang, Y.; Shetty, K.; Mishra, B.; Mishra, L. *Sci. STKE.* **2007**, *39*, cm1.

Therapeutics, Targets, and Chemical Biology

Cancer Research

Identification of EP4 as a Potential Target for the Treatment of Castration-Resistant Prostate Cancer Using a Novel Xenograft Model

Naoki Terada[1], Yosuke Shimizu[1], Tomomi Kamba[1], Takahiro Inoue[1], Atsushi Maeno[1], Takashi Kobayashi[1], Eijiro Nakamura[1,6], Toshiyuki Kamoto[1,7], Toshiya Kanaji[8], Takayuki Maruyama[8], Yoshiki Mikami[2], Yoshinobu Toda[3], Toshiyuki Matsuoka[4], Yasushi Okuno[5], Gozoh Tsujimoto[5], Shuh Narumiya[4], and Osamu Ogawa[1]

Abstract

More effective therapeutic approaches for castration-resistant prostate cancer (CRPC) are urgently needed, thus reinforcing the need to understand how prostate tumors progress to castration resistance. We have established a novel mouse xenograft model of prostate cancer, KUCaP-2, which expresses the wild-type androgen receptor (AR) and which produces the prostate-specific antigen (PSA). In this model, tumors regress soon after castration, but then reproducibly restore their ability to proliferate after 1 to 2 months without AR mutation, mimicking the clinical behavior of CRPC. In the present study, we used this model to identify novel therapeutic targets for CRPC. Evaluating tumor tissues at various stages by gene expression profiling, we discovered that the prostaglandin E receptor EP4 subtype (EP4) was significantly upregulated during progression to castration resistance. Immunohistochemical results of human prostate cancer tissues confirmed that EP4 expression was higher in CRPC compared with hormone-naïve prostate cancer. Ectopic overexpression of EP4 in LNCaP cells (LNCaP-EP4 cells) drove proliferation and PSA production in the absence of androgen supplementation *in vitro* and *in vivo*. Androgen-independent proliferation of LNCaP-EP4 cells was suppressed when AR expression was attenuated by RNA interference. Treatment of LNCaP-EP4 cells with a specific EP4 antagonist, ONO-AE3-208, decreased intracellular cyclic AMP levels, suppressed PSA production *in vitro*, and inhibited castration-resistant growth of LNCaP-EP4 or KUCaP-2 tumors *in vivo*. Our findings reveal that EP4 overexpression, via AR activation, supports an important mechanism for castration-resistant progression of prostate cancer. Furthermore, they prompt further evaluation of EP4 antagonists as a novel therapeutic modality to treat CRPC. *Cancer Res; 70(4); 1606–15. ©2010 AACR.*

Introduction

Prostate cancer is one of the most frequently diagnosed cancers in the Western world (1). Because prostate cancer development is initially dependent on androgens, medical or surgical castration is the mainstay therapy for patients with advanced prostate cancer. However, most patients ultimately relapse after a period of initial response to this therapy, progressing to castration-resistant prostate cancer (CRPC). Effective therapeutic approaches for CRPC are extremely limited. Treatment with docetaxel was established as a new standard of care for CRPC patients (2). However, it is not curative, and optimal timing of administration remains controversial. Consequently, it is highly desirable to explore new therapeutic strategies based on detailed molecular mechanisms for the development of castration resistance in prostate cancer.

The generation of suitable *in vivo* models is critical to better understand the processes associated with the development and progression of prostate cancer. We have previously reported a novel prostate cancer xenograft model named KUCaP-1 (previously referred to as KUCaP; ref. 3). KUCaP-1 tumors harbor the W741C mutant androgen receptor (AR), regress soon after castration in mice, and do not regrow with long-term follow-up (4). We have now established another novel xenograft model named KUCaP-2 using locally recurrent CRPC specimens derived from a different patient. The KUCaP-2 tumors harbor wild-type AR, regress soon after castration, and restore their ability to proliferate after 1 to 2 months without AR mutation. As the sequential changes of the xenograft resemble the clinical behavior of prostate cancer, this model may provide an excellent system to

Authors' Affiliations: [1]Department of Urology, Kyoto University Graduate School of Medicine; [2]Department of Diagnostic Pathology, Kyoto University Hospital; [3]Anatomical Center, Kyoto University Graduate School of Medicine; [4]Department of Pharmacology, Faculty of Medicine, Kyoto University; [5]Department of Genomic Drug Discovery Science, Kyoto University Graduate School of Pharmaceutical Sciences, Kyoto, Japan; [6]Department of Medical Oncology, Dana-Farber Cancer Institute, Boston, Massachusetts; [7]Department of Urology, Miyazaki University, Miyazaki, Japan; and [8]Development Research Laboratories, Research Headquarters, Ono Pharmaceutical Co., Ltd., Osaka, Japan

Corresponding Author: Osamu Ogawa, Department of Urology, Kyoto University Graduate School of Medicine, 54, Shogoinkawahara-cho, Sakyo-ku, Kyoto 606-8507, Japan. Phone: 81-75-751-3325; Fax: 81-75-761-3441; E-mail: ogawao@kuhp.kyoto-u.ac.jp.

doi: 10.1158/0008-5472.CAN-09-2984

study the mechanisms associated with castration-resistant progression of prostate cancer and to evaluate new treatment modalities for CRPC.

In KUCaP-2, prostaglandin E receptor EP4 subtype (EP4) expression significantly increased with the development of castration resistance. We explored the function of EP4 in prostate cancer cells as a potential target for the treatment of CRPC.

Materials and Methods

Generation of xenograft model. Clinical materials were used after informed consent was obtained, according to protocols approved by the institutional review board at Kyoto University Hospital. All experiments involving laboratory animals were done in accordance with the Guideline for Animal Experiments of Kyoto University. Local recurrent tumors after radical prostatectomy were resected trans-urethrally, minced into 20 to 30 mm^3 tumor bits, and transplanted s.c. into 5-wk-old male nude mice (Charles River Japan) with 50 μL of Matrigel (Becton Dickinson) injected around the implant. The KUCaP-2 xenograft was established ~10 mo after the first inoculation. The xenograft tumors were extracted and transplanted to several mice without Matrigel. Ninety percent of the tumor was serially transplantable.

Sequence analysis. Genomic DNA from the xenograft tissue was extracted and all of the exons of the *AR* gene were sequenced as previously reported (3).

Tissue sampling and DNA microarray analysis. The mice bearing KUCaP-2 tumors were castrated and the sequential changes in tumor volume were analyzed as previously reported (3). Serum samples were obtained at sacrifice to measure prostate-specific antigen (PSA) values. Xenograft tissues of KUCaP-2 were collected during various stages and total RNA was isolated and purified using the RNeasy Mini Kit (Qiagen). Changes in gene expression were analyzed using DNA microarray analysis with an Affymetrix Human Genome U133 Plus2.0.

Real-time PCR. cDNA was synthesized from total RNA using a First-Strand cDNA Synthesis Kit (Amersham Pharmacia Biotech). Real-time PCR was performed using SYBR green PCR Master Mix (Applied Biosystems) and monitored using GeneAmp 5700 (Applied Biosystems) in triplicate. The thermal cycling conditions were 95°C for 15 s, 60°C for 30 s, and 72°C for 30 s. The values were normalized to the levels of amplified glyceraldehyde-3-phosphate dehydrogenase (GAPDH). The sequences of primers were as follows: EP4, 5′-GGAAATGACCAGGCCAAGAC-3′ (sense) and 5′-CAACCCTGGACCTCACACCTA-3′ (antisense); PSA, 5′-GGAAATGACCAGGCCAAGAC-3′ (sense) and 5′-CAACCCTGGACCTCACACCTA-3′ (antisense); AR, 5′-CTTCACCAATGTCAACTCCA-3′ (sense) and 5′-TCATTCGGACACACTGGCTG-3′ (antisense); and GAPDH, 5′-GAATATAATCCCAAGCGGTTTG-3′ (sense) and 5′-ACTTCACATCACAGCTCCCC-3′ (antisense).

Antibodies and reagents. Anti-AR (C-19: sc-815) and anti-PSA (C-19: sc7638) antibodies were obtained from Santa Cruz Biotechnology. Anti–β-actin antibody (AC-15: ab6276) was purchased from Abcam. Anti-EP4 antibody (COOH terminus: 101775) for Western blotting was obtained from Cayman Chemical and anti-EP4 antibody (N terminus: LS-A3898) for immunohistochemistry was obtained from MBL International. The EP4-specific antagonist ONO-AE3-208 was provided by Ono Pharmaceutical Co. (5). 5α-Dihydrotestosterone was purchased from Sigma. Forskolin, an activator of adenylate cyclase, and dibutyryl cyclic AMP (dbcAMP), a cAMP analogue, were purchased from Nacalai Tesque. H-89, a cAMP-dependent protein kinase (PKA) inhibitor, was obtained from Biomol International. An expression vector, pcDNA3.1-EP4, was constructed by inserting the cDNA of human EP4, digested from a cloning vector, pBluescript-EP4 (6), into *Hin*dIII-*Bam*HI sites of pcDNA3.1(−). Vectors were transfected into the cells using Lipofectamine 2000 reagent (Invitrogen) and transfectants were selected by geneticin (Nacalai Tesque).

Western blotting and immunohistochemistry. Western blotting was performed with each primary antibody (AR, 1:400; PSA, 1:400; EP4 1:700; β-actin, 1:5,000) as previously reported (7). Immunohistochemistry was performed by standard indirect immunoperoxidase procedures using each primary antibody (AR, 1:100; PSA, 1:100; EP4 1:400), and the reaction was enhanced by microwave only in EP4 immunohistochemistry. Hormone-naïve prostate cancer (HNPC) tissues were derived from radical prostatectomy specimens of localized prostate cancer patients as tissue microarrays constructed as previously reported (8, 9). CRPC tissue samples were local tumors obtained from patients undergoing transurethral resection or autopsy. The expression intensity was graded as none, weak, moderate, and strong by a clinical pathologist (Y.M.) who was blind to the clinicopathologic data. The grading was determined based on the intensity of staining for at least 20% of the cancer cells.

Cell culture. The prostate cancer cell lines LNCaP, DU145, and PC3 were obtained from the American Type Culture Collection, passaged for fewer than 6 mo after resuscitation. The cells were routinely cultured in RPMI 1640 (Invitrogen) supplemented with 10% fetal bovine serum. For androgen-depleted conditions, cells were cultured in phenol red–free RPMI 1640 (Invitrogen) supplemented with 10% charcoal-stripped fetal bovine serum (CSFBS; Hyclone). To analyze the cell proliferation *in vitro*, 1.0×10^5 cells per well were seeded into six-well plates and grown for indicated days, and then cell numbers were counted in triplicate by a hemocytometer. For the assessment of *in vivo* tumor growth, 0.5×10^7 to 1.0×10^7 cells were inoculated with 100 μL Matrigel in the flank region of 5-wk-old male nude mice, and tumor volumes were measured once weekly.

RNA interference. AR knockdown was performed using stealth RNAi [stAR(1);HSS100620 and stAR(2);HSS100619] compared with control nonspecific stealth RNAi (stCtr;12935-400) purchased from Invitrogen. Cells were seeded at 5.0×10^5 per well in six-well plates and incubated for 24 h. Each 160 pmol of stealth RNAi was transfected using Lipofectamine 2000 reagent.

Luciferase assay. Cells were seeded at 1.5×10^5 per well in 24-well plates and were transiently cotransfected with 250 ng